Credit portfolio losses with climate change factors

Oriol Tubella-Domingo and Luis Ortiz-Gracia

UBIREA | Institut de Recerca en Economia Aplicada Regional i Pública

UBIREA | Institut de Recerca en Economia Aplicada Regional i Pública
UNIVERSITAT DE BARCELONA

WEBSITE: www.ub.edu/irea/ • CONTACT: irea@ub.edu

The Research Institute of Applied Economics (IREA) in Barcelona was founded in 2005, as a research institute in applied economics. Three consolidated research groups make up the institute: AQR, RISK and GiM, and a large number of members are involved in the Institute. IREA focuses on four priority lines of investigation: (i) the quantitative study of regional and urban economic activity and analysis of regional and local economic policies, (ii) study of public economic activity in markets, particularly in the fields of empirical evaluation of privatization, the regulation and competition in the markets of public services using state of industrial economy, (iii) risk analysis in finance and insurance, and (iv) the development of micro and macro econometrics applied for the analysis of economic activity, particularly for quantitative evaluation of public policies.

Abstract

In this work, we consider the problem of computing risk measures of a credit portfolio via the evaluation of the characteristic function of the loss variable. We propose a new methodology to obtain the characteristic function of the loss distribution when the dependence structure is driven by either the Gaussian or t-copula model. This new approach relies on a quadrature method based on Shannon wavelets and the cardinal sine function. It works out extremely well for the one-factor and the multi-factor model when, in the second case, a moderate number of risk factors are considered. Then, we compare with some of the state-of-the-art methods to perform the same task, and we get much better results in terms of execution time and accuray. As quadrature methods are affected by the curse of dimensionality, we further introduce a simulation approach to evaluate the characteristic function in the case of multi-factor models with many risk factors. The simulation is based on lowdiscrepancy Monte Carlo sequences. A broad set of numerical examples illustrate the efficiency of our methodology. We conclude our work with a real portfolio where the exposures are taken from the European Investment Bank, and we incorporate climate change-related factors into the analysis. This study highlights the practical relevance of our methodology for assessing credit risk in portfolios exposed to emerging environmental challenges.

AMS subject classifications. 65T60, 91B05, 91G40, 91G60

Keywords: Credit risk; multi-factor models; Gaussian copula; t-copula; Climate change; Shannonwavelets

Authors:

Oriol Tubella-Domingo. Departament d'Econometria, Estad´ıstica i Economia Aplicada, Universitat de Barcelona (UB), Av. Diagonal, 690, 08034 Barcelona, Spain

Luis Ortiz-Gracia. Corresponding Author**.** RISKcenter, Institut de Recerca en Economia Aplicada (IREA), Universitat de Barcelona (UB), Av. Diagonal, 690, 08034 Barcelona, Spain. luis.ortiz-gracia@ub.edu

1 Introduction

Pursuant to the Basel Accords [3, 4], banks are subject to regulatory capital requirements that mandate the assessment and management of risks inherent in their business operations. Although commercial banks currently offer a broad spectrum of financial products, credit risk, defined as the risk of loss resulting from a counterparty's failure to fulfill contractual obligations, remains the predominant source of financial risk. The principal regulatory metric for quantifying credit risk is the Value-at-Risk (VaR), typically calculated over a one-year horizon, that estimates the potential loss at the 99.9% confidence level of the credit loss distribution, thereby capturing extreme but plausible loss events and informing the capital reserves required to mitigate such risks. Under the Basel II (see [4]) and Basel III (see [3]) frameworks, financial institutions are required to calculate regulatory capital for credit risk. This calculation is based on the Asymptotic Single Risk Factor (ASRF) model, which is derived from the Vasicek one-factor model. In this Gaussian framework, default events are driven by a single latent systematic factor, typically representing the state of the economy, which is assumed to follow a normal distribution plus some idiosyncratic noise. There are two main drawbacks in this model. On the one hand, it assumes a portfolio of a large number of relatively small exposures and, on the other hand, all risks affecting the borrowers are modeled with only one systematic risk factor. This model can underestimate risks in the presence of exposure concentrations as it was shown in [17]. To account for various factors that might affect a portfolio of borrowers, multi-factor models have been introduced. Although these factors have traditionally been related to economic variables, they can be associated to climate change risk factors (see [8]).

Climate change introduces a complex and evolving set of risks for banks and financial institutions impacting both, their short-term operations, and long-term stability. As discussed in [5], these risks fall into two main categories: physical risks and transition risks. The first type arises from the direct impact of climate-related events such as floods, hurricanes, wildfires, and droughts that might make the value of collateral held by banks to decline. This increases the likelihood of loan defaults and reduces asset values, weakening the financial institution's balance sheet. On the other hand, as the world moves toward a low-carbon economy, changes in policy, regulation, technology and consumer preferences can impact the profitability of certain industries. Banks with large exposures to fossil fuel companies or carbon-intensive sectors may see a decline in asset values or creditworthiness. This can affect lending, investment portfolios, and long-term strategic planning. All these problematics fall into the category of transition risks. All in all, multi-factor models can be seen as a powerful tool to take into account these risks factors alongside the economic ones.

Monte Carlo (MC) simulation is still the most common approach for computing risk measures under the one-factor and multi-factor models. The flexibility of the method is the main reason why MC is attractive for financial companies, but simulation becomes in general very time-consuming as the portfolio size increases or even when a moderate number of factors are considered in the multi-factor case. Different results can be found in the literature for dealing with multi-factor Gaussian copula models. Some logarithmic limits for the loss distribution under two different limiting regimes was provided in [9] but, again, both limits rely on letting the size of the portfolio increase. A granularity adjustment was presented by [14], and then applied to a multi-factor framework by [20] to compute risk measures. Finally, [10] developed the quadratic transform approximation (QTA) that provides a closed-form approximation to the Laplace transform of the loss variable in multi-factor Gaussian copula models. While the regulatory framework relies on Gaussian approaches, alternative models based on different distributions can be explored to capture tail dependence and contagion risk. To be more precise, we put our attention into the one-factor and multi-factor t-copula models. We refer the reader to [7], where the authors compute risk measures with dependence structure among obligors driven by t-copula moldels. The characteristic function is evaluated for the t-copula case by conditioning on the chi-squared factor and then applying repeatedly the QTA method to the Gaussian case. Once the characteristic function is obtained, a Haar wavelets-based inversion method (see [15]) is used to recover the loss distribution function for calculating the VaR and the Expected Shortfall (ES) risk measures.

In the present work, we develop novel methods to compute the characteristic function of the loss variable for one-factor and multi-factor Gaussian and t-copula models. In the case of either one-factor or multi-factor model with a moderate number of factors, we propose an accurate and fast quadrature

method based on Shannon wavelets and the cardinal sine function, and we call it SINC-WA method. When the multi-factor model contains a high number of factors, we show that low-discrepancy Monte Carlo sequences work out well and outperform existing methods. In that situation, our proposed method is called QMC-WA. The acronym SINC stems from the cardinal sine function, or sinc in short, while QMC refers to quasi MC methods. We assess the efficienty of our methods by comparing with some of the most relevant numerical methods encountered in the literature: GH-WA (Gauss-Hermite) from [15], and GHGL-WA (Gauss-Hermite, Gauss-Laguerre) and QTA-WA from [7]. When to use each of them will be clear in the numerical experiments section. In all cases, the inversion of the characteristic function is carried out by the Haar wavelets-based method of [15] and that is why we use the acronym WA. It is worth mentioning that QTA originally developed in [10] was used in that work along with a numerical Laplace transform inversion method. In the present work, we use the QTA equipped with WA as in [7], since the performance is much better. The benchmark for comparisons will be always MC. Specifically, the contributions of this paper are as follows.

- Within the one-factor model framework, we compute the VaR and the ES risk measures under the Gaussian and the t-copula model, where a numerical quadrature based on Shannon wavelets expansions and the sinc function is employed to compute the characteristic function of the loss variable. This integration method was used in the context of option pricing (see [11]) but, to the best of our knowledge, never before when computing credit risk measures. The numerical experiments show that this approach achieves high efficiency compared to GH-WA, which is the standard integration method for the Gaussian copula model in [15]. When it comes to compute the risk measures under the t-copula model, our method shows impressive accuracy and execution time when comparing with GHGL-WA used in [7] for solving the two-dimensional integral involved in the characteristic function evaluation. The accuracy of all the methods used in this work is assessed by means of the relative error, considering MC as the benchmark. For the t-copula model, the SINC-WA method achieves a reduction in the relative error ranging from a factor of 10 to 100, being particularly well suited for a low number of degrees of freedom of the chi-squared variable, when state-of-the-art methods tend to fail.

- Within the multi-factor setting, we propose two different strategies to approximate the characteristic function, depending on the number of factors. For a model with a moderate number of factors we consider a multi-dimensional quadrature version of SINC-WA method, whereas for a high number of factors we consider the QMC-WA method.

- For a multi-factor model, matrices of factor loadings with large norms hamper the satisfactory use of the QTA-WA method, while SINC-WA and QMC-WA are naturally capable of providing accurate results. For the multi-factor t-copula model, the SINC-WA method achieves an impressive reduction in the relative error in the range of 10 to 10^4 when compared to QTA-WA, where this last method produces nonsensical results.

- We provide a theoretical error analysis allowing to determine the parameters of the SINC-WA method, so that we have full control on its use.

- We provide results of risk measures of a credit portfolio with real data, where the exposures are taken from the European Investment Bank (EIB).

The work is organised as follows. In Section 1.1 we present the managerial relevance of this work by pointing out to actionable insights for policymakers and risk managers. In Section 2, we review the one-factor and multi-factor Gaussian and t-copula models for credit risk, and their corresponding characteristic functions are detailed in Section 3. We put forward the inversion step of the characteristic function in Section 4. Section 5 is the core of the theoretical research, where a novel integration method for numerically evaluating the characteristic function is presented. Section 6 is devoted to the numerical experiments and a case study based on real data. Finally, Section 7 concludes.

1.1 Actionable insights for policymakers and risk managers

Factor Gaussian models are widely used by banks to manage their credit risk at portfolio level. They are employed to calculate regulatory capital under Pillar I, as well as economic capital under Pillar II of Basel Accords. While regulatory capital is measured with the ASRF model, the economic capital is typically calculated with costly MC simulations. Whether one- or multi-factor models, they all rely on the Gaussian copula for driving the dependence structure among the obligors.

The novel method put forward in this work, allows for tail dependence and risk contagion by means of the t-copula model. For the one-factor and the multi-factor case, we provide numerical methods where all the parameters are known beforehand, making the results reliable for real-world practice. It is not only the robustness and accuracy what makes this methodology interesting in practice, but also the impressive execution time. Stress tests can be carried out with many repetitions over different scenarios and large real portolios in short computing time, allowing the managers and policymakers to assess the impact in terms of risk of a change in one or more capital parameters. Climate-related risk factors are naturally incorporated in the multi-factor Gaussian and t-copula models framework, providing this way a tool for measuring transition and physical risks in credit portfolios.

2 Portfolio credit risk models

In this section, we present the one-factor and multi-factor Gaussian (Section 2.1) and t-copula (Section 2.2) models for credit risk. These are the two models that we are going to use throughout this work, whether in their single-factor or multi-factor versions.

Consider a credit portfolio consisting of N obligors. For $j = 1, \dots, N$ we denote by τ_j a random variable representing the time that the j-th obligor defaults and whose marginal distribution function $F_j(t) = P(\tau_j \leq t)$ is known. Any obligor j can be characterized by the three well-known capital parameters, the *exposure at default* (EAD), the *loss given default* (LGD), and the *probability of default* (PD), denoted by E_j, Λ_j, and P_j respectively. The individual loss variable associated to each borrower is given by

$$L_j = E_j \Lambda_j \mathbb{1}_{\{\tau_j \leq t\}}, \tag{1}$$

where t denotes time, typically one year. In particular, $E_j\Lambda_j$ is the effective exposure with respect to obligor j, and it represents the part of the total exposure that cannot be recovered in case of default. In practice, E_j is known beforehand, and to take into account uncertainty in the recovery rate, the LGD Λ_j might be modelled as a random variale, and its distribution may depend on time. In this work, we will assume a deterministic loss given default of 100%, that is, $\Lambda_j = 1$ for every $j = 1, \dots, N$. Considering this, we can express the aggregated default losses of the portfolio at time t as,

$$L(t) := \sum_{j=1}^{N} L_j = \sum_{j=1}^{N} E_j \mathbb{1}_{\{\tau_j \leq t\}}. \tag{2}$$

It remains to establish a model for individual defaults as well as the dependence structure among the obligors. Regarding the modelling of individual defaults, we rely on the Merton model, where default takes place whenever the asset value of obligor j falls below its debt. For the dependence structure, we consider the Gaussian copula and the t-copula: while the first lays the foundations of Basel II credit risk models, the second takes into account tail dependence.

2.1 Gaussian copula model

We start this section by presenting the one-factor Gaussian copula model, where the value of the assets (or firm-value) of the j-th obligor at time t, denoted by X_j, is driven by a common systematic factor Z that is shared by all obligors, and an idiosyncratic factor ϵ_j, unique for every obligor,

$$X_j = \sqrt{\rho_j} Z + \sqrt{1 - \rho_j} \epsilon_j, \tag{3}$$

where Z and ϵ_j are *i.i.d.* standard normally distributed random variables for all j and $\rho_1, \cdots, \rho_N \in [0, 1]$ are correlation parameters. In case that $\rho_j = \rho$ for all obligors, the parameter ρ is called the common

asset correlation. In Merton's model, obligor j defaults when its firm-value at the considered time horizon t falls below some threshold level α_j gien by $\alpha_j := \Phi^{-1}(P_j) = \Phi^{-1}(F_j(t))$ where Φ^{-1} denotes the inverse of the standard normal cumulative distribution function (CDF) and, in practice, P_j is estimated from empirical data.

Multi-factor models aim to model complicated correlation structures. The d-factor Gaussian copula model assumes that the correlation among X_j is introduced through $d \times 1$ vector $\mathbf{Z} = (Z_1,\ Z_2, \ldots, Z_d)^T$ of independent standard normal random variables representing systematic risk factors such that,

$$X_j = \mathbf{a}_j^T \mathbf{Z} + b_j \epsilon_j, \quad j = 1, \ldots, N, \tag{4}$$

where $\mathbf{a}_j = [a_{j1}, a_{j2}, \ldots, a_{jd}]^T$ is a $d \times 1$ vector of real constants satisfying $\mathbf{a}_j^T \mathbf{a}_j < 1$ and ϵ_j are standard normally distributed random variables representing the idiosyncratic risks, independent of each other for every obligor and independent of $\mathbf{Z}$. In a matricial form, expression (4) can be written as,

$$\begin{bmatrix} X_1 \\ X_2 \\ \vdots \\ X_N \end{bmatrix} = \begin{bmatrix} a_{11} \\ a_{21} \\ \vdots \\ a_{N1} \end{bmatrix} Z_1 + \begin{bmatrix} a_{12} \\ a_{22} \\ \vdots \\ a_{N2} \end{bmatrix} Z_2 + \cdots + \begin{bmatrix} a_{1d} \\ a_{2d} \\ \vdots \\ a_{Nd} \end{bmatrix} Z_d + \begin{bmatrix} b_1\epsilon_1 \\ b_2\epsilon_2 \\ \vdots \\ b_N\epsilon_N \end{bmatrix}. \tag{5}$$

From (5) is it clear that each Z_j might affect all (or a certain group of) obligors. However, the idiosyncratic factor ϵ_j just affects the obligor j. The matrix $\mathbf{A} = (a_{ij})_{1 \le i \le N, 1 \le j \le d}$, is called the *matrix of factor loadings* and we assume it constant over time. The constant b_n, being the factor loading of the idiosyncratic risk factor, is chosen so that each X_j has unit variance, i.e., $b_j = \sqrt{1 - (a_{j1}^2 + a_{j2}^2 + \cdots + a_{jd}^2)}$ which ensures again that $X_j \sim \mathcal{N}(0, 1)$.

The one-factor Gaussian copula model is employed by banks to calculate the regulatory capital for credit risk under Pilar I of Basel Accords. Under certain assumptions on the portfolio size and its granularity, the VaR can be readily obtained by means of a closed-form formula, at the cost of underestimating the risk in the presence of exposure concentration, which typically occurs in practice (see for instance [12] or [15]). Then, under Pillar II of Basel Accords, banks compute the economic capital to account for exposure or sectorial (or geographical) concentration by means of the multi-factor Gaussian copula model and the costly MC simulation.

2.2 t-copula model

It is well established in the literature (see for example [16]) that the Gaussian copula exhibits no tail dependence, meaning that, if one obligor defaults in extreme circumstances the chance of another defaulting at the same time is underestimated. As a result, the Gaussian copula model underestimates risks and portfolio tail losses particularly in stressed environments as the model cannot realistically capture contagion effects or systemic crises. To overcome these limitations, another alternative dependence structures among obligors have been proposed. One of the most studied is the t-copula model, which differs from the Gaussian copula in the fact that the latent variables follow the t-distribution rather than the Gaussian distribution. The one-factor t-copula model reads,

$$X_j = \sqrt{\frac{\nu}{Y}} \left(\sqrt{\rho_j} Z + \sqrt{1 - \rho_j} \epsilon_j \right), \tag{6}$$

where $Y \sim \chi^2_\nu$ i.e, Y is a random variable that follows a chi-squared distribution with ν degrees of freedom and also independent of Z. In this case, every obligor j defaults if $X_j < \Phi_\nu^{-1}(P_j)$, where Φ_ν^{-1} denotes the quantile function of the univariate t-distribution with ν degrees of freedom.

The multi-factor counterpart reads,

$$X_j = \sqrt{\frac{\nu}{Y}} \Big(\mathbf{a}_j^T \mathbf{Z} + b_j \epsilon_j \Big), \quad j = 1, \ldots, N, \tag{7}$$

where $\mathbf{a}_j, \mathbf{Z}$ and b_j are defined as in Section 2.1, and Y is independent of $\mathbf{Z}$.

In Section 3, we give the details for obtaining the characteristic functions corresponding to the models presented in this section. Unfortunately, any of them can be expressed in analytical form and then, numerical methods must be employed for their evaluation. We tackle that task in Section 5.

3 Characteristic function of the loss variable

Given the loss random variable L, we define its characteristic function $\varphi_L : \mathbb{R} \to \mathbb{C}$ of L as $\varphi_L(\omega) := \mathbb{E}[e^{-i\omega L}]$, that is, the probabilistic counterpart of the Fourier transfrom of the loss density function $f_L(x)$. For the Gaussian copula model, and following [10], it is clear from (4) that given a realization of the vector of systematic risk factors $\mathbf{Z}$ obligors become independent as they are just affected by the idiosyncratic factor. We therefore can obtain the so-called conditional probability of default of obligor j conditional on the realization $\mathbf{Z} = \mathbf{z}$ of the systematic risk factors $\mathbf{Z}$,

$$p_j(\mathbf{z}) := \mathbb{P}(X_j \leq \Phi^{-1}(P_j)|\mathbf{Z} = \mathbf{z}) = \Phi\left(\frac{\Phi^{-1}(P_j) - \mathbf{a}_j^T\mathbf{z}}{b_j}\right).$$

Note that $\mathbb{P}(X_j \leq \Phi^{-1}(P_j)|\mathbf{Z} = \mathbf{z}) = \mathbb{P}(\tau_j \leq t|\mathbf{Z} = \mathbf{z})$ is the conditional probability of default within some fixed time t. Using the conditional independence argument, we obtain,

$$\mathbb{E}[\mathrm{e}^{-i\omega L}|\mathbf{Z}] = \prod_{j=1}^{N} \mathbb{E}[e^{-i\omega E_j \mathbb{1}_{\{\tau_j \leq t\}}}|\mathbf{Z}] = \prod_{j=1}^{N}\left(1 + \left(\mathrm{e}^{-i\omega E_j} - 1\right)\Phi\left(\frac{\Phi^{-1}(P_j) - \mathbf{a}_j^T\mathbf{Z}}{b_j}\right)\right). \tag{8}$$

Finally, using the law iterated expectations, the characteristic function φ_L of L is therefore given by,

$$\varphi_L(\omega) = \mathbb{E}\left[e^{-i\omega L}\right] = \mathbb{E}\left[\mathbb{E}\left[\, e^{-i\omega L} \mid \mathbf{Z}\right]\right] = \int_{\mathbb{R}^d} f_{\boldsymbol{Z}}(\boldsymbol{z}) \prod_{j=1}^{N}\left(1 + \left(\mathrm{e}^{-i\omega E_j} - 1\right)\Phi\left(\frac{\Phi^{-1}(P_j) - \mathbf{a}_j^T\mathbf{z}}{b_j}\right)\right) d\mathbf{z}. \tag{9}$$

where $f_{\boldsymbol{Z}}(\mathbf{z})$ is the d-dimensional standard Gaussian density, meaning that the characteristic function can be recovered from (8) integrating over the factors $\mathbf{Z}$. In a more compact way, for a fixed ω, we denote for a given $\mathbf{v} \in \mathbb{R}^d$ and for every obligor $j = 1, \ldots, N$ the mappings $\mathbf{v} \mapsto g_j(\mathbf{v})$ as

$$g_j(\mathbf{v}; \omega) := 1 + \left(\mathrm{e}^{-i\omega E_j} - 1\right)\Phi\left(\frac{\Phi^{-1}(P_j) - \mathbf{a}_j^T\mathbf{v}}{b_j}\right), \quad \mathbf{v} \in \mathbb{R}^d. \tag{10}$$

We denote by,

$$g(\mathbf{v}; \omega) = \prod_{j=1}^{N} g_j(\mathbf{v}; \omega), \tag{11}$$

and rewrite the characteristic function (9) for the Gaussian copula model as follows,

$$\varphi_L(\omega) = \mathbb{E}\left[\prod_{j=1}^{N} g_j(\mathbf{Z}; \omega)\right] = \mathbb{E}\left[g(\mathbf{Z}; \omega)\right] = \int_{\mathbb{R}^d} f_{\boldsymbol{Z}}(\boldsymbol{z}) g(\mathbf{z}; \omega) d\mathbf{z}. \tag{12}$$

For the t-copula model, we need to condition on both $\mathbf{Z}$ and Y. In this case, the default probability of obligor j conditional on realizations of the factors $\mathbf{Z} = \mathbf{z}$ and $Y = y$ is given by,

$$\begin{aligned} p_j(\mathbf{z}, y) &:= \mathbb{P}(X_j < \Phi_\nu^{-1}(P_j) \mid \mathbf{Z} = \mathbf{z}, Y = y) = \mathbb{P}\left(\sqrt{\frac{\nu}{y}}\left(\mathbf{a}_j^T\mathbf{z} + b_j\epsilon_j\right) < \Phi_\nu^{-1}(P_j)\right) \\ &= \mathbb{P}\left(\epsilon_j < \frac{\sqrt{\frac{y}{\nu}}\Phi_\nu^{-1}(P_j) - \mathbf{a}_j^T\mathbf{z}}{b_j}\right) = \Phi\left(\frac{\sqrt{\frac{y}{\nu}}\Phi_\nu^{-1}(P_j) - \mathbf{a}_j^T\mathbf{z}}{b_j}\right). \end{aligned}$$

In particular, we note that given $Y = y$ we get the Gaussian copula model with changed marginal conditional default probability. Again, using conditional independence, the equivalent of expression (9)

reads,

$$\varphi_L(\omega) = \mathbb{E}\left[e^{-i\omega L}\right] = \mathbb{E}\left[\mathbb{E}\big[\, e^{-i\omega L} \;\big|\; \mathbf{Z}, Y\big]\right] = \mathbb{E}\left[\prod_{j=1}^{N}\left(1 + \left(\mathrm{e}^{-i\omega E_j} - 1\right)\Phi\left(\frac{\sqrt{\frac{y}{\nu}}\Phi_\nu^{-1}(P_j) - \mathbf{a}_j^T\mathbf{z}}{b_j}\right)\right)\right] \tag{13}$$

$$= \int_{\mathbb{R}^d\times[0,\infty]} \prod_{j=1}^{N}\left(1 + \left(\mathrm{e}^{-i\omega E_j} - 1\right)\Phi\left(\frac{\sqrt{\frac{y}{\nu}}\Phi_\nu^{-1}(P_j) - \mathbf{a}_j^T\mathbf{z}}{b_j}\right)\right) f_{\boldsymbol{Z}}(\boldsymbol{z}) f_Y(y) d\mathbf{z}dy, \tag{14}$$

where $f_Y(y)$ is the chi-square probability density function with ν degrees of freedom, that is,

$$f_Y(y) = \frac{1}{2^{\nu/2}\Gamma(\nu/2)} y^{\nu/2-1} e^{-y/2}, \quad y > 0, \tag{15}$$

$\Gamma(\cdot)$ denotes the gamma function. For the t-copula model, let us define,

$$g_j(\mathbf{v}, y; \omega) := 1 + \left(\mathrm{e}^{-i\omega E_j} - 1\right)\Phi\left(\frac{\sqrt{\frac{y}{\nu}}\Phi_\nu^{-1}(P_j) - \mathbf{a}_j^T\mathbf{v}}{b_j}\right), \quad \mathbf{v} \in \mathbb{R}^d. \tag{16}$$

As before, we can denote by,

$$g(\mathbf{v}, y; \omega) = \prod_{j=1}^{N} g_j(\mathbf{v}, y; \omega), \tag{17}$$

and rewrite the characteristic function as,

$$\varphi_L(\omega) = \int_{\mathbb{R}^d\times[0,\infty]} f_{\boldsymbol{Z}}(\boldsymbol{z}) f_Y(y) \prod_{j=1}^{N} g_j(\mathbf{z}, y; \omega) d\mathbf{z}dy = \int_{\mathbb{R}^d\times[0,\infty]} f_{\boldsymbol{Z}}(\boldsymbol{z}) f_Y(y) g(\mathbf{z}, y; \omega) d\mathbf{z}dy. \tag{18}$$

Throughout this article, we will use the notation g interchangeably to denote both expressions (11) and (17), depending on whether we are working under a Gaussian or t-copula model. It will be clear from the context which definition is being used in each case.

It is worth remarking that, for one-factor Gaussian and t-copula models, the characteristic functions are obtained by replacing the random vector $\boldsymbol{Z}$ by the random variable Z in expression (9) and expression (18), respectively.

4 The inversion step and risk measures computation

Once the characteristic function $\varphi_L(\omega)$ is available, it remains to carry out the inversion step to calculate the risk measures. We choose here the Fourier inversion method called WA, which is based on Haar wavelets and it shows extremely accurate approximation properties for a piecewise constant CDF, like the one that appears naturally in this credit risk context (see [15] for details of the original WA method, and [7, 19] for comparisons with other methods). For sake of completeness, we briefly recall the WA method.

Let F_L be the CDF of L. Without loss of generality we assume that the sum of the exposures E_n is one, this is, $\sum_{n=1}^{N} E_n = 1$. Then,

$$F_L(x) = \begin{cases} F^c(x), & \text{if } 0 \le x \le 1, \\ 0, & \text{if } x > 1, \end{cases} \tag{19}$$

for a certain $F^c(x)$ defined in $[0, 1]$. Then, the Fourier transform $\hat{F}^c(\omega)$ of F^c is given by,

$$\hat{F}^c(\omega) = \frac{\varphi_L(\omega) - e^{-i\omega}}{i\omega}. \tag{20}$$

We aim at recovering $F^c(x)$ from its Fourier transform $\hat{F}^c(\omega)$. The idea behind the WA method is expanding $F^c(x)$ in terms of Haar wavelets, where the coefficients of the expansion are computed using $\hat{F}^c(\omega)$. The following section elaborates on the key ideas regarding a general function approximation with wavelets.

4.1 Multi-resolution analysis and wavelets

Consider the space $L^2(\mathbb{R}) = \{f : \int_{-\infty}^{+\infty} |f(x)|^2\, dx < \infty\}$. For simplicity we can view this set as the set of functions $f(x)$ which get small in magnitude rapidly as x goes to plus and minus infinity. A general structure for wavelets in $L^2(\mathbb{R})$ is called a *Multi-resolution Analysis* (MRA). We start with a family of closed nested subspaces,

$$... \subset V_{-2} \subset V_{-1} \subset V_0 \subset V_1 \subset V_2 \subset ...,$$

in $L^2(\mathbb{R})$ where,

$$\bigcap_{m\in\mathbb{Z}} V_m = \{0\}, \qquad \overline{\bigcup_{m\in\mathbb{Z}} V_m} = L^2(\mathbb{R}),$$

and,

$$f(x) \in V_m \iff f(2x) \in V_{m+1}.$$

If these conditions are met, then there exists a function $\phi \in V_0$ such that $\{\phi_{j,k}\}_{k\in\mathbb{Z}}$ is an orthonormal basis of V_j, where,

$$\phi_{j,k}(x) = 2^{j/2}\phi(2^j x - k).$$

The function ϕ, called the *father function*, generates an orthonormal basis for each V_j subspace. For any $f \in L^2(\mathbb{R})$ a projection map of $L^2(\mathbb{R})$ onto V_m,

$$\mathcal{P}_m : L^2(\mathbb{R}) \to V_m,$$

is defined by means of,

$$\mathcal{P}_m f(x) = \sum_{k\in\mathbb{Z}} c_{m,k}\phi_{m,k}(x), \tag{21}$$

where $c_{m,k} = \int_{-\infty}^{+\infty} f(x)\phi_{m,k}(x)dx$ are the scaling coefficients. The right-hand side of (21) gives a sum in terms of the scaling functions $\phi_{m,k}$. Considering higher m values (i.e., when more terms are used), the truncated series representation of the function f improves.

4.2 Haar wavelets expansion

The WA method is based on a wavelets expansion of the CDF of L using Haar wavelets as scaling functions. In this case, the father function is given by,

$$\phi(x) = \begin{cases} 1, & \text{if } 0 \le x < 1, \\ 0, & \text{otherwise,} \end{cases}$$

Using these wavelets, V_j is the set of $L^2(\mathbb{R})$ functions which are non-zero only on each interval of the form $[\frac{k}{2^j}, \frac{k+1}{2^j})$ for all integers k. In our case, we approximate $F^c(x)$ of expression (19) by a finite combination of Haar scaling functions at a fixed scale of approximation m,

$$F^c(x) \approx F^c_m(x) := \sum_{k=0}^{2^m-1} c_{m,k}\phi_{m,k}(x), \tag{22}$$

with convergence in the $L^2(\mathbb{R})$-norm. Observe that we cover the domain of definition of F^c, which is $[0, 1]$, by the union of non-overlapping supports of $\phi_{m,k}$. If we define,

$$Q_m(z) := \frac{2^{m/2}\hat{F}^c\left(2^m i \ln(z)\right)}{\hat{\phi}(i\ln(z))},$$

then, the coefficients of expression (22) can be numerically computed,

$$c_{m,k} \approx \frac{1}{r^k J}\sum_{j=0}^{J-1} Q_m(re^{i\frac{2\pi}{J}j})e^{-i2\pi\frac{k}{J}j}, \tag{23}$$

where $J = 2^m$ and $r = 0.9995$ (see [18] for details on the choice of r).

Once the coefficients $c_{m,k}$ are obtained, the calculation of both the VaR and the ES given a confidence level $\alpha \in (0,1)$ (typically close to 1) is straightforward. In particular,

$$\mathrm{VaR}_\alpha(L) := \inf\{l \in \mathbb{R} : F_L(l) \geq \alpha\} \approx l_\alpha^m := \frac{2\bar{k}+1}{2^{m+1}}, \tag{24}$$

for $\bar{k}$ such that $\mathrm{VaR}_\alpha(L) \in [\frac{\bar{k}}{2^m}, \frac{\bar{k}+1}{2^m}]$ and $\frac{\alpha}{2^{m/2}} \in \left[c_{m,\bar{k}}, c_{m,\bar{k}+1}\right]$, since $F^c\left(\mathrm{VaR}_\alpha(L)\right) \geq \alpha$, and,

$$\mathrm{ES}_\alpha := \frac{1}{1-\alpha}\int_{l_\alpha}^{+\infty} x f_L(x)dx \approx \frac{1}{1-\alpha}\left(1 - \alpha l_\alpha - \frac{1}{2^{\frac{m}{2}+1}}c_{m,\bar{k}} - \frac{1}{2^{m/2}}\sum_{k=\bar{k}+1}^{2^m-1} c_{m,k}\right), \tag{25}$$

where $l_\alpha := \mathrm{VaR}_\alpha(L)$ is replaced by the VaR value l_α^m calculated at scale m in (24). We refer the reader to Section 4.2 of [7] for more details.

5 Numerical evaluation of the characteristic function

As mentioned in the introduction, we present in this work the novel SINC-WA numerical method for evaluating the characteristic functions of Section 3. The accuracy and speed of this method is compared with other numerical methods that perform the same task and, for this reason, we briefly detail each of them. For all of them, the benchmark is always MC, which is considered the exact value for both VaR and ES.

5.1 GH-WA and GHGL-WA methods

In order to calculate the risk measures, the characteristic function $\varphi_L(\omega)$ must be evaluated in many points ω, and this translates into the computation of integrals for each value of ω. For a one-factor model, that is, $d = 1$, we use for comparisons the GH-WA and GHGL-WA methods from [7, 15], to deal with Gaussian and t-copula models, respectively. In particular, for the Gaussian copula model (GH-WA method), as the only systematic factor Z follows a standard normal distribution, we can make use of a Gauss-Hermite quadrature,

$$\varphi_L(\omega) \approx \frac{1}{\sqrt{2\pi}}\sum_{i=1}^{N_{\mathrm{GH}}} w_i \prod_{j=1}^{N} g_j(x_i;\omega) = \frac{1}{\sqrt{2\pi}}\sum_{i=1}^{N_{\mathrm{GH}}} w_i g(x_i;\omega), \tag{26}$$

where N_{GH} is the number of sample points used. The $x_i, i = 1, 2, \cdots, N_{\mathrm{GH}}$, are the roots of the Hermite polynomial $H_{N_{\mathrm{GH}}}(x)$ of degree N_{GH}, and the associated weights w_i are given by $w_i = \frac{c}{H_{N_{\mathrm{GH}}-1}(x_i)H'_{N_{\mathrm{GH}}}(x_i)}$, for a normalizing constant c.

For the case of the t-copula (GHGL-WA method), we have two nested integrals,

$$\varphi_L(\omega) = \int_0^\infty f_Y(y)\left(\int_{\mathbb{R}} f_Z(z)\prod_{j=1}^{N}\left(1 + \left(\mathrm{e}^{-i\omega E_j} - 1\right)\Phi\left(\frac{\sqrt{\frac{y}{\nu}}\Phi_\nu^{-1}(P_j) - a_j z}{b_j}\right)\right)dz\right)dy. \tag{27}$$

We solve the inner integral by means of a Gauss-Hermite quadrature as explained before. For the outer integral, we use a generalized Gauss–Laguerre quadrature,

$$\varphi_L(\omega) \approx \frac{1}{\sqrt{2\pi}}\frac{1}{\Gamma\left(\frac{\nu}{2}\right)}\sum_{i=1}^{N_{\mathrm{GL}}} w_i^{\mathrm{GL}}\sum_{j=1}^{N_{\mathrm{GH}}} w_j^{\mathrm{GH}}\prod_{j=1}^{N} g_j(x_j^{\mathrm{GH}}, 2y_i^{\mathrm{GL}};\omega) = \frac{1}{\sqrt{2\pi}}\frac{1}{\Gamma\left(\frac{\nu}{2}\right)}\sum_{i=1}^{N_{\mathrm{GL}}} w_i^{\mathrm{GL}}\sum_{j=1}^{N_{\mathrm{GH}}} w_j^{\mathrm{GH}} g(x_j^{\mathrm{GH}}, 2y_i^{\mathrm{GL}};\omega), \tag{28}$$

where the pairs $(x_j^{\mathrm{GH}}, w_j^{\mathrm{GH}})$ and $(y_i^{\mathrm{GL}}, w_i^{\mathrm{GL}})$ represent the nodes and weights of Gauss-Hermite and Gauss-Laguerre quadratures, respectively. In the case of Gauss-Laguerre, the weights are given by,

$$w_i^{\mathrm{GL}} = \frac{\Gamma(N_{\mathrm{GH}} + \nu/2)y_i^{\mathrm{GL}}}{N_{\mathrm{GH}}!(N_{\mathrm{GH}}+1)^2\left[L_{N_{\mathrm{GH}}+1}^{(\nu/2-1)}(y_i^{\mathrm{GL}})\right]^2},$$

where y_i^{GL} are the roots of the generalized Laguerre polynomials $L_{N_{\mathrm{GH}}}^{(\nu/2-1)}$.

It is worth underlining that, despite that many programming languages have both nodes and weights tabulated, the direct computation might be time-consuming and numerically unstable if a large number of points are needed.

5.2 QTA-WA method

We give now a brief review of the QTA method of [9] for the multi-factor Gaussian copula that was extended to the multi-factor t-copula in [7].

For the Gaussian copula, we define,

$$\tilde{g}_j(v;\omega) := 1 + \left(\mathrm{e}^{-i\omega E_j} - 1\right) \Phi\left(\frac{\Phi^{-1}(P_j) + v\sqrt{\mathbf{a}_j^T \mathbf{a}_j}}{b_j}\right), \ v \in \mathbb{R}, \tag{29}$$

and we rewrite the conditional expectation as follows,

$$\mathbb{E}\big[\, e^{-i\omega L} \mid \mathbf{Z}\big] = \prod_{j=1}^{N} \tilde{g}_j(V_j;\omega) = e^{\sum_{j=1}^{N} \ln g_j(V_j;\omega)}, \quad \text{where} \quad V_j = \frac{-\mathbf{a}_j^T \mathbf{Z}}{\sqrt{\mathbf{a}_j^T \mathbf{a}_j}}. \tag{30}$$

The key idea is to approximate each term $\ln g_j(V_j;\omega)$ by a quadratic function of V_j,

$$\ln\, g_j(V_j;\omega) \approx \alpha_j(\omega) + \beta_j(\omega) V_j + \eta_j(\omega) V_j^2,$$

where $\alpha_j(\omega), \beta_j(\omega)$ and $\eta_j(\omega)$ are complex values. Here we emphasize the dependence on ω, since we need to estimate the three coefficients for every obligor and for every ω. Then, we can approximate the characteristic function as,

$$\begin{aligned}
\varphi_L(\omega) &= \mathbb{E}\left[e^{\sum_{j=1}^{N} \ln g_j(V_j;\omega)}\right] \approx \mathbb{E}\left[e^{\sum_{j=1}^{N} \alpha_j(\omega) + \beta_j(\omega) V_j + \eta_j(\omega) V_j^2}\right] \\
&= \mathbb{E}\left[\mathrm{e}^{c(\omega) + \boldsymbol{g}^T(\omega)\boldsymbol{Y} + \boldsymbol{Z}^T \boldsymbol{H}(\omega) \boldsymbol{Z}}\right] = \frac{1}{\sqrt{\det(\boldsymbol{I} - 2\boldsymbol{H}(\omega))}} e^{c(\omega) + \boldsymbol{g}(\omega)^T (\boldsymbol{I} - 2\boldsymbol{H}(\omega))^{-1} \boldsymbol{g}(\omega)/2},
\end{aligned} \tag{31}$$

where,

$$c(\omega) = \sum_{j=1}^{N} \alpha_j(\omega), \quad \boldsymbol{g}(\omega) = -\sum_{j=1}^{N} \frac{\beta_j(\omega) \boldsymbol{a}_j}{\sqrt{\boldsymbol{a}_j^T \boldsymbol{a}_j}}, \ \text{ and } \ \boldsymbol{H}(\omega) = \sum_{j=1}^{N} \eta_j(\omega) \frac{\boldsymbol{a}_j \boldsymbol{a}_j^T}{\boldsymbol{a}_j^T \boldsymbol{a}_j}. \tag{32}$$

We note that $c(\omega) \in \mathbb{C}$, $\boldsymbol{g}(\omega) \in \mathbb{C}^d$ is a vector, $\boldsymbol{H}(\omega) \in \mathbb{C}^{d \times d}$ is a matrix, and $\boldsymbol{I}$ is the d-dimensional identity matrix. The last equally in (31) is derived in Proposition 1 of [9], and we compute the coefficients $(\alpha_j(\omega), \beta_j(\omega), \eta_j(\omega))$ with the weighted least-squares method.

For the t-copula model, the key idea is conditioning on $Y = y$ in the model of expression (7), and then reducing the problem to the Gaussian copula model with changed marginal default probability. By doing that, we end up with the approximation,

$$\begin{aligned}
\varphi_L(\omega) &\approx \int_0^{+\infty} f_Y(y) \mathbb{E}\left[e^{c(\omega,y) + \boldsymbol{g}^T(\omega,y)\boldsymbol{Y} + \boldsymbol{Y}^T \boldsymbol{H}(\omega,y) \boldsymbol{Y}}\right] dy \\
&= \frac{1}{2^{\frac{\nu}{2}} \Gamma\left(\frac{\nu}{2}\right)} \int_0^{+\infty} y^{\frac{\nu}{2}-1} e^{-\frac{y}{2}} \frac{1}{\sqrt{\det(\boldsymbol{I} - 2\boldsymbol{H}(\omega,y))}} e^{c(\omega,y) + \boldsymbol{g}^T(\omega,y)(\boldsymbol{I} - 2\boldsymbol{H}(\omega,y))^{-1} \boldsymbol{g}(\omega,y)/2} dy,
\end{aligned} \tag{33}$$

and compute the integral in expression (33) by a generalized Gauss-Laguerre quadrature.

5.3 SINC-WA method

We give here the fundamentals of the methodoloy for the one-factor Gaussian and t-copula models. We will provide the explicit formulae for the three-factor Gaussian copula as well as for the two-factor t-copula in the numerical experiments section, since they are natural extensions of the one-factor counterparts.

Shannon wavelets (see [6] for more details) are understood within the multi-resolution analysis framework of Section 4.1, where, in this case, the father wavelet is given by the sinc function, defined as,

$$\text{sinc}(x) = \begin{cases} \frac{\sin(\pi x)}{\pi x}, & \text{if } x \neq 0, \\ 1, & \text{if } x = 0. \end{cases} \tag{34}$$

A set of Shannon scaling functions in the subspace V_m is defined as,

$$\phi_{m,k}(x) = 2^{m/2} \frac{\sin(\pi(2^m x - k))}{\pi(2^m x - k)}, \quad k \in \mathbb{Z}. \tag{35}$$

It is clear that for $m = k = 0$, we have the father wavelet,

$$\phi(x) = \text{sinc}(x).$$

The following therorems lay the basis of the methodology put forward in Section 5.3.1 and Section 5.3.2, and they will be used repeatedly. They underline the relation between the decay of the modulus of the Fourier transform of a certain function with the approximation properties of Shannon wavelet expansions.

Theorem 1 (Theorem 1.3.2 of [22]). *Let f be defined on $\mathbb{R}$ and let its Fourier transform, denoted by $\hat{f}$, be such that, for some positive constant d,*

$$|\hat{f}(\xi)| = \mathcal{O}\left(e^{-d|\xi|}\right), \quad \xi \to \pm\infty \ . \tag{36}$$

Then, as $a \to 0$,

$$\frac{1}{a}\int_{\mathbb{R}} f(y)\mathcal{S}(k,a)(y)dy - f(ka) = \mathcal{O}\left(e^{-\frac{\pi d}{a}}\right), \tag{37}$$

where $\mathcal{S}(k,a)(y) := sinc\left(\frac{y}{a} - k\right)$, for $k \in \mathbb{Z}$.

Theorem 2 (Lemma 3 of [13]). *Let $f \in L^2(\mathbb{R})$ and denote by $\hat{f}$ its Fourier transform. Let us consider a projection as in (21). Then, the error $\varepsilon_P(x) := |f(x) - \mathcal{P}_m f(x)|$ is uniformly bounded by,*

$$\varepsilon_P(x) \leq \frac{1}{2\pi}\int_{|\xi|>2^m\pi} |\hat{f}(\xi)|d\xi, \ \textit{for all } x \in \mathbb{R}. \tag{38}$$

Theorem 3 (Theorem 2 of [11]). *Let f be defined on $\mathbb{R}$ and denote by $\hat{f}$ its Fourier transform. Then, for $a = \frac{1}{2^m}$,*

$$\left|\frac{1}{a}\int_{\mathbb{R}} f(y)\mathcal{S}(k,a)(y)dy - f(ka)\right| \leq \frac{1}{2\pi}\int_{|\xi|>\frac{\pi}{a}} |\hat{f}(\xi)|d\xi \tag{39}$$

where again $\mathcal{S}(k,a)(y) := sinc\left(\frac{y}{a} - k\right)$ for $k \in \mathbb{Z}$.

5.3.1 Gaussian copula model

Consider the one-dimension integral resulting from expression (12) when taking $d = 1$,

$$\varphi_L(\omega) = \int_{\mathbb{R}} f_Z(z) \prod_{j=1}^{N} \left(1 + \left(\mathrm{e}^{-i\omega E_j} - 1\right)\Phi\left(\frac{\Phi^{-1}(P_j) - a_j z}{b_j}\right)\right) dz = \int_{\mathbb{R}} f_Z(z) g(z;\omega) dz. \tag{40}$$

We start by considering an approximation by means of Shannon wavelets at scale m of the standard normal density function $f_Z(z)$ following the theory of Section 4.1.

Proposition 1. *Let $f_{Z,m}(z) := \sum_{k\in\mathbb{Z}} c_{m,k}\phi_{m,k}(z)$ be the Shannon wavelets approximation at scale m of $f_Z(z)$, where $c_{m,k} = \int_{-\infty}^{+\infty} f_Z(z)\phi_{m,k}(z)dz$. Then, for all $\epsilon > 0$, and for all $z \in \mathbb{R}$, $|f_Z(z) - f_{Z,m}(z)| < \epsilon$ if,*

$$m > \frac{\ln\left(\text{erf}^{-1}(1 - \epsilon\sqrt{2\pi})\right) - \ln(\pi)}{\ln(2)} + \frac{1}{2}, \tag{41}$$

where $\text{erf}^{-1}(\cdot)$ is the inverse error function. Further, the coefficients $c_{m,k}$ can be well approximated by $\bar{c}_{m,k} := 2^{-\frac{m}{2}} f_Z\left(\frac{k}{2^m}\right)$, and,

$$|c_{m,k} - \bar{c}_{m,k}| < \epsilon, \ \textit{for all } k \ \in \mathbb{Z}. \tag{42}$$

Proof. By Theorem 2,

$$|f_Z(z) - f_{Z,m}(z)| \leq \frac{1}{2\pi} \int_{|\xi|>2^m\pi} |\hat{f}_Z(\xi)| d\xi = \frac{1}{2\pi} \int_{|\xi|>2^m\pi} e^{-\xi^2/2} d\xi = \frac{1}{\pi} \int_{2^m\pi}^{+\infty} e^{-\xi^2/2} d\xi = \frac{1 - \mathrm{erf}(2^{m-\frac{1}{2}}\pi)}{\sqrt{2\pi}}. \tag{43}$$

Solving the inequality $\frac{1-\mathrm{erf}(2^{m-\frac{1}{2}}\pi)}{\sqrt{2\pi}} < \epsilon$ yields the result in expression (41). The approximation error in expression (42) follows straightforwardly from Theorem 3. □

Once the scale of approximation m is set, it remains to truncate the infinitie series expansion of Shannon wavelets into a finite number of terms,

$$f_Z(z) \approx \bar{f}_{Z,m}(z) := \sum_{k=k_1}^{k_2} \bar{c}_{m,k} \phi_{m,k}(z), \tag{44}$$

where the selection of k_1 and k_2 is detailed in Section 5.3.3.

Finaly, we replace $f_Z(z)$ by $\bar{f}_{Z,m}(z)$ in expression (40), and we end up with,

$$\varphi_L(\omega) \approx \bar{\varphi}_L(\omega) := \frac{1}{2^{m/2}} \sum_{k=k_1}^{k_2} f_Z\left(\frac{k}{2^m}\right) \int_{\mathbb{R}} \phi_{m,k}(z) g(z;\omega) dz \approx \frac{1}{2^m} \sum_{k=k_1}^{k_2} f_Z\left(\frac{k}{2^m}\right) g\left(\frac{k}{2^m};\omega\right), \tag{45}$$

where we approximate $\int_{\mathbb{R}} \phi_{m,k}(z) g(z;\omega) dz$ by $\frac{1}{2^{m/2}} g\left(\frac{k}{2^m};\omega\right)$. Based on a heuristic argument, we conclude that this last approximation is highly accurate, although we have not proved whether the hypothesis of Theorem 3 are satisfied.

5.3.2 t-copula model

We proceed similarly as in the former section to compute the characteristic function for the one-factor t-copula model. We consider the two-dimension integral resulting from expression (18) when taking $d = 1$,

$$\varphi_L(\omega) = \int_{\mathbb{R}\times[0,\infty]} \prod_{j=1}^{N} \left(1 + \left(\mathrm{e}^{-i\omega E_j} - 1\right) \Phi\left(\frac{\sqrt{\frac{y}{\nu}}\Phi_\nu^{-1}(P_j) - a_j z}{b_j}\right)\right) f_Z(z) f_Y(y) dz dy, \tag{46}$$

and we replace $f_Z(z)$ by $\bar{f}_{Z,m}(z)$ in expression (46) as in Section 5.3.1, yielding,

$$\varphi_L(\omega) \approx \bar{\varphi}_L(\omega) := \sum_{k=k_1}^{k_2} \bar{c}_{m,k} \int_{\mathbb{R}\times[0,\infty]} g\left(z, y; \omega\right) \phi_{m,k}(z) f_Y(y) dz dy. \tag{47}$$

If we integrate with respect to the variable z and apply Theorem 3 to that integral, we end up with,

$$\bar{\varphi}_L(\omega) \approx \bar{\bar{\varphi}}_L(\omega) := \frac{1}{2^{\frac{m}{2}}} \sum_{k=k_1}^{k_2} \bar{c}_{m,k} \int_0^{+\infty} g\left(\frac{k}{2^m}, y; \omega\right) f_Y(y) dy. \tag{48}$$

Taking into account that Y follows a chi-squared distribution with ν degrees of freedom, and making the change of variables $t = \ln(y)$, we obtain,

$$\begin{aligned} \bar{\bar{\varphi}}_L(\omega) &= \frac{1}{2^{\frac{m}{2}}} \cdot \frac{1}{2^{\nu/2}\Gamma\left(\frac{\nu}{2}\right)} \sum_{k=k_1}^{k_2} \bar{c}_{m,k} \int_0^{+\infty} y^{\frac{\nu}{2}-1} e^{-\frac{y}{2}} g\left(\frac{k}{2^m}, y; \omega\right) dy \\ &= \frac{1}{2^{\frac{m}{2}}} \cdot \frac{1}{2^{\nu/2}\Gamma\left(\frac{\nu}{2}\right)} \sum_{k=k_1}^{k_2} \bar{c}_{m,k} \int_{-\infty}^{+\infty} e^{\frac{\nu}{2}t - \frac{1}{2}e^t} g\left(\frac{k}{2^m}, e^t; \omega\right) dt. \end{aligned} \tag{49}$$

Let us define $f(t) := e^{\frac{\nu}{2}t - \frac{1}{2}e^t}$, and consider its approximation in terms of Shannon wavelets at the scale of approximation $\tilde{m}$, that is,

$$f(t) \approx f_{\tilde{m}}(t) := \sum_{k\in\mathbb{Z}} c_{\tilde{m},k}\phi_{\tilde{m},k}(t), \tag{50}$$

where $c_{\tilde{m},k} = \int_{-\infty}^{+\infty} f(t)\phi_{\tilde{m},k}(t)dt$. The Fourier transform $\hat{f}(\xi)$ of $f(t)$ can be computed explicitly in terms of the gamma function $\Gamma(\cdot)$, yielding,

$$\hat{f}(\xi) = 2^{(\frac{\nu}{2}-i\xi)}\Gamma\left(\frac{\nu}{2} - i\xi\right). \tag{51}$$

It can be shown that $|\hat{f}(\xi)|$ decays exponentially when $\xi \to \pm\infty$, and Theorem 1 guarantees that the approximation,

$$c_{\tilde{m},k} \approx \tilde{c}_{\tilde{m},k} := 2^{-\frac{\tilde{m}}{2}} f\left(\frac{k}{2^{\tilde{m}}}\right), \tag{52}$$

has an error which decays exponentially as well. The details on the computation of the Fourier transform of $f(t)$, and the exponential decay of the modulus of its Fourier transform are given in Proposition 2.

Proposition 2. *By definition,*

$$\hat{f}(\xi) = \int_{-\infty}^{+\infty} e^{\frac{\nu}{2}t - \frac{1}{2}e^t} e^{-i\xi t}dt = \int_0^{+\infty} e^{\frac{\nu}{2}\ln(y) - \frac{1}{2}e^{\ln(y)}} e^{-i\xi\ln(y)}\frac{1}{y}dy = \int_0^{+\infty} y^{s-1}e^{\frac{-y}{2}}dy, \tag{53}$$

where $s = \frac{\nu}{2} - i\xi$. After performing the change of variables $u = \frac{y}{2}$ we get (51) for $\xi \in \mathbb{R}$.

We need to study $|\hat{f}(\xi)| = 2^{\frac{\nu}{2}}|\Gamma\left(\frac{\nu}{2} - i\xi\right)|$. We should first note that as $\nu > 0$ then $\mathrm{Re}(\frac{\nu}{2} - i\xi) > 0$ so all the evaluating points lie in the semiplane $\{z \in \mathbb{C} : \mathrm{Re}(z) > 0\}$ where the Gamma function is holomorphic, hence $Arg\left(\frac{\nu}{2} - i\xi\right) = arctan\left(\frac{-2\xi}{\nu}\right) \in \left(\frac{-\pi}{2}, \frac{\pi}{2}\right)$ depending on the sign of ξ. Using Stirling's formula for the Gamma function (see Chapter 6 of [1]) for $\xi \to \infty$, and omitting the asymptotic $O\left(\frac{1}{z}\right)$ terms for $\ln\Gamma(z)$, we have that,

$$\ln\Gamma\left(\frac{\nu}{2} - i\xi\right) \approx \frac{1}{2}\ln(2\pi) + \left(\frac{\nu-1}{2} - i\xi\right)\ln\left(\frac{\nu}{2} - i\xi\right) - \left(\frac{\nu}{2} - i\xi\right). \tag{54}$$

Recall that the complex logarithm can be defined as $\ln(z) = \ln|z| + iArg(z)$, then, when $\xi \to \pm\infty$, we approximate $\ln\left(\frac{\nu}{2} - i\xi\right)$ by $\ln|\xi| - isgn(\xi)\frac{\pi}{2}$, where sgn denotes the sign function. The product in the right hand side of (54), reads,

$$\left(\frac{\nu-1}{2} - i\xi\right)\ln\left(\frac{\nu}{2} - i\xi\right) \approx \left(\frac{\nu-1}{2} - i\xi\right)\left(\ln|\xi| - isgn(\xi)\frac{\pi}{2}\right) \tag{55}$$

$$= \frac{\nu-1}{2}\ln|\xi| - isgn(\xi)\frac{\pi}{2}\frac{\nu-1}{2} - i\xi\ln|\xi| - |\xi|\frac{\pi}{2}, \tag{56}$$

and,

$$\ln\Gamma\left(\frac{\nu}{2} - i\xi\right) \approx \frac{1}{2}\ln(2\pi) + \frac{\nu-1}{2}\ln|\xi| - |\xi|\frac{\pi}{2} - \frac{\nu}{2} + i\left(-sgn(\xi)\frac{\pi}{2}\frac{\nu-1}{2} - \xi\ln|\xi| + \xi\right). \tag{57}$$

Finally, the approximation,

$$|\Gamma\left(\frac{\nu}{2} - i\xi\right)| = |e^{\ln\Gamma\left(\frac{\nu}{2}-i\xi\right)}| = e^{\mathrm{Re}\left(\ln\Gamma\left(\frac{\nu}{2}-i\xi\right)\right)} \approx e^{\frac{1}{2}\ln(2\pi) + \frac{\nu-1}{2}\ln|\xi| - |\xi|\frac{\pi}{2} - \frac{\nu}{2}} = \sqrt{2\pi}|\xi|^{\frac{\nu-1}{2}}e^{-|\xi|\frac{\pi}{2} - \frac{\nu}{2}}, \tag{58}$$

confirms the exponential decay of $|\hat{f}(\xi)|$.

However, for practical reasons on the determination of $\tilde{m}$, it would be convenient to consider an approximation $f^a(t)$ of $f(t)$, facilitating this way the integration of the right hand side of Theorem 3.

We consider a second-order Taylor expansion of the exponent $\Phi(t) = \frac{\nu}{2}t - \frac{1}{2}e^t$ of $f(t)$ around its maximum. Specifically, we use the function $f^a(y)$ defined as,

$$f(t) \approx f^a(t) := e^{\Phi(t_0) - \frac{\nu}{4}(t-t_0)^2} = \nu^{\frac{\nu}{2}}e^{-\frac{\nu}{2}}e^{-\frac{\nu}{4}(t-t_0)^2}, \tag{59}$$

where $t_0 = \ln(\nu)$. The Fourier transform $\hat{f}^a(\xi)$ of $f^a(t)$ can be obtained in closed-form,

$$\hat{f}^a(\xi) = 2\sqrt{\frac{\pi}{\nu}}\nu^{\frac{\nu}{2}}e^{-\frac{\nu}{2}}e^{-i\xi\ln(\nu)}e^{-\frac{\xi^2}{\nu}}. \tag{60}$$

Proposition 3. *For all $\epsilon > 0$, and,*

$$\tilde{m} > \frac{1}{\ln(2)}\ln\left(\frac{\sqrt{\nu}}{\pi}\,\mathrm{erf}^{-1}\left(1 - \frac{\epsilon}{\nu^{\frac{\nu}{2}}e^{-\frac{\nu}{2}}}\right)\right), \tag{61}$$

where $\mathrm{erf}^{-1}(\cdot)$ is the inverse error function, the integral of the right hand side of Theorem 3 satisfies,

$$\frac{1}{2\pi}\int_{|\xi|>2^m\pi} |\hat{f}^a(\xi)|d\xi < \epsilon. \tag{62}$$

Proof. From expression (60),

$$\frac{1}{2\pi}\int_{|\xi|>2^m\pi} |\hat{f}^a(\xi)|d\xi = \frac{1}{2\pi}\int_{|\xi|>2^{\tilde{m}}\pi} 2\sqrt{\frac{\pi}{\nu}}\nu^{\frac{\nu}{2}}e^{-\frac{\nu}{2}}e^{-\frac{\xi^2}{\nu}}d\xi = \nu^{\frac{\nu}{2}}e^{-\frac{\nu}{2}}\left(1 - \mathrm{erf}\left(\frac{2^{\tilde{m}}\pi}{\sqrt{\nu}}\right)\right). \tag{63}$$

It is possible to obtain an error of magnitude ϵ we need to impose $\nu^{\frac{\nu}{2}}e^{-\frac{\nu}{2}}\left(1 - \mathrm{erf}\left(\frac{2^{\tilde{m}}\pi}{\sqrt{\nu}}\right)\right) < \epsilon$, and this concludes the proof. □

Once the scale of approximation $\tilde{m}$ is set, it remains to truncate the infinitie series expansion of Shannon wavelets in expression (50) into a finite number of terms, and replace the coeficients $c_{\tilde{m},k}$ by their approximations in expression (52),

$$f(t) \approx \tilde{f}_{\tilde{m}}(t) := \sum_{k=\tilde{k}_1}^{\tilde{k}_2} \tilde{c}_{\tilde{m},k}\phi_{\tilde{m},k}(t), \tag{64}$$

where the selection of $\tilde{k}_1$ and $\tilde{k}_2$ is detailed in Section 5.3.3.

Finally, we replace $f(t)$ by $\tilde{f}_{\tilde{m}}(t)$ in expression (49), and we end up with,

$$\bar{\tilde{\varphi}}_L(\omega) \approx \tilde{\varphi}_L(\omega) := \frac{1}{2^{\frac{m}{2}}}\cdot\frac{1}{2^{\nu/2}\Gamma\left(\frac{\nu}{2}\right)}\sum_{k=k_1}^{k_2}\bar{c}_{m,k}\sum_{\tilde{k}=\tilde{k}_1}^{\tilde{k}_2}\tilde{c}_{\tilde{m},\tilde{k}}\int_{-\infty}^{+\infty}\phi_{\tilde{m},\tilde{k}}(t)g\left(\frac{k}{2^m}, e^t; \omega\right)dt \tag{65}$$

$$= \frac{1}{2^m}\cdot\frac{1}{2^{\frac{\tilde{m}}{2}}}\cdot\frac{1}{2^{\nu/2}\Gamma\left(\frac{\nu}{2}\right)}\sum_{k=k_1}^{k_2} f_Z\left(\frac{k}{2^m}\right)\sum_{\tilde{k}=\tilde{k}_1}^{\tilde{k}_2} f\left(\frac{\tilde{k}}{2^{\tilde{m}}}\right)\int_{-\infty}^{+\infty}\phi_{\tilde{m},\tilde{k}}(t)g\left(\frac{k}{2^m}, e^t; \omega\right)dt \tag{66}$$

$$\approx \tilde{\bar{\varphi}}_L(\omega) := \frac{1}{2^m}\cdot\frac{1}{2^{\tilde{m}}}\cdot\frac{1}{2^{\nu/2}\Gamma\left(\frac{\nu}{2}\right)}\sum_{k=k_1}^{k_2} f_Z\left(\frac{k}{2^m}\right)\sum_{\tilde{k}=\tilde{k}_1}^{\tilde{k}_2} f\left(\frac{\tilde{k}}{2^{\tilde{m}}}\right)g\left(\frac{k}{2^m}, e^{\frac{\tilde{k}}{2^{\tilde{m}}}}; \omega\right). \tag{67}$$

The last approximation for g is based on a heuristic argument, like in Section 5.3.1.

5.3.3 Domain truncation

Regarding the selection of $k_1, k_2, \tilde{k}_1$ and $\tilde{k}_2$, we aim to minimize the loss of mass in the tails of $f_Z(z)$ and $f(t)$, respectively, due to the domain truncation. We denote by $[a, b]$ the trunctated domain, and we select a and b such that,

$$P(X \leq a) = \frac{\alpha}{2}, \quad \text{and,} \quad P(X \geq b) = \frac{\alpha}{2},$$

where a total tail mass of α is lost, corresponding $\alpha/2$ to each tail, and X represents either the standard normal distribution Z of Section 5.3.1 or the chi-squared distribution Y of Section 5.3.2.

Then, given the scales of approximaton m and $\tilde{m}$, we set,

$$k_1 = 2^m \cdot \lfloor a \rfloor, k_2 = 2^m \cdot \lceil b \rceil, \tilde{k}_1 = 2^{\tilde{m}} \lfloor \ln(a) \rfloor, \tilde{k}_2 = 2^{\tilde{m}} \lceil \ln(b) \rceil,$$

where $\lfloor \cdot \rfloor$ and $\lceil \cdot \rceil$ denote the floor and ceil functions, respectively.

Note that we use the logarithmic transformation for $\tilde{k}_1$ and $\tilde{k}_2$, since we want to truncate the domain of the function $f(t) = e^{t\frac{\nu}{2} - \frac{1}{2}e^t}$, obtained after the change of variables $t = \ln(y)$, which is a monotone transformation.

6 Numerical experiments

In this section, we aim to compare the results obtained for the VaR and the ES using the novel SINC-WA method with different methodologies presented in Section 5. MC simulation will be used to compute the VaR and ES at the regulatory 99.9% confidence level in every experiment, with these results serving as a benchmark for comparisons. In the one-factor case of Section 6.1, we will consider both the Gaussian and the t-copula models, and we will assess the performance of SINC-WA when compared with GH-WA, GHGL-WA and QTA-WA. For multi-factor models of Section 6.2, we will propose two different approaches depending on the number of factors of the model. For a moderate number of factors, we will implement a multi-dimensional SINC-WA method, for both the Gaussian and t-copula models, and assess its performance when comparing with QTA-WA. For a large number of factors, we use QMC-WA, which is a simulation approach based on low-discrepancy MC sequences. Finally, we put forward in Section 6.3 a case study with real data.

All the numerical experiments were carried out using Python in a computer equipped with an AMD Ryzen 5 3600 3.60 GHz 6-Core Processor and 32 GB of RAM memory.

6.1 One-factor models

We start our numerical experiments with a one-factor model with a fixed common correlation parameter $\rho = 0.15$ for every obligor. Table 1 shows the parameters corresponding to our first portfolio P0. When computing credit risk measures, it is well-known that small or concentrated portfolios are particularly challenging cases, since the regulatory ASRF model relies on the non realistic assumptions of large and diversified portfolios. We will consider for our numerical examples portfolios of different sizes showing name concentration, which is typically measured with the Herfindahl-Hirschman Index (HHI).

Portfolio	**N**	$\boldsymbol{E_n}$	$\boldsymbol{P_n}$	$\boldsymbol{\rho}$	**HHI**
P0	100	$C \cdot \frac{1}{n}$	0.005	0.15	0.061

Table 1: Portfolio P0. The constant C is calculated such that $\sum_{j=1}^{N} E_j = 1$. MC is run with a sample size of 10^7 for the systematic factor Z.

6.1.1 Gaussian copula model

Given the specified portfolio, we first compute the VaR and ES under the Gaussian copula model with MC, GH-WA and QTA-WA methods. Results are shown in Table 2. We can observe that relative errors are similar in both cases, but the CPU time employed by GH-WA with the number of quadrature points specified by N_{GH} ranges from 0.01 to 0.05 seconds, while QTA-WA needs 0.71 seconds. The GH quadratures were calculated with the function `hermegauss` from Numpy's `HermiteE` class.

Now we compute the same risk measures applying our SINC-WA method. We need to select the parameters m, k_1, k_2 for the approximation of the normal density function. Regarding the scale of approximation, we follow Proposition 1 with $\epsilon = 10^{-3}$ and $\epsilon = 10^{-5}$, obtaining $m = 0$ and $m = 1$, respectively. Just for the sake of comparison, we have also computed risk measures for $m = 2$. With respect to the truncation values k_1 and k_2, we selected them as explained in Section 5.3.3. We assume a total loss of $\alpha = 0.00001$ in the tails of the distribution. We get $a \approx -4.417, b \approx 4.417$, and $k_1 = 2^m \lfloor a \rfloor =$

Method	Parameters	P0		Time
		VaR	ES	
MC		0.210928	0.239850	113.97
	N_{GH}	**VaR Error**	**ES Error**	
QTA-WA		2.2711×10^{-3}	1.8040×10^{-2}	0.71
GH-WA	7	2.3588×10^{-3}	6.9056×10^{-3}	
	8	2.3588×10^{-3}	7.1935×10^{-3}	
	11	2.3588×10^{-3}	7.0845×10^{-3}	
	13	2.3588×10^{-3}	7.0671×10^{-3}	
	21	2.3588×10^{-3}	7.0688×10^{-3}	
	25	2.3588×10^{-3}	7.0688×10^{-3}	
	41	2.3588×10^{-3}	7.0688×10^{-3}	

Table 2: Relative errors with respect to MC when computing VaR and ES with QTA-WA and GH-WA. The CPU time is measured in seconds.

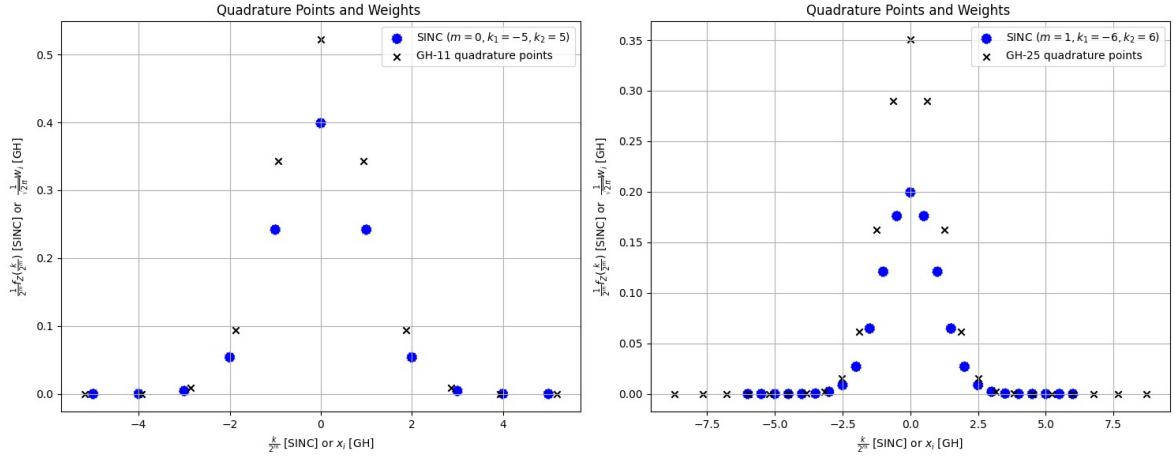

Figure 1: Quadrature nodes and weights for SINC-WA (dots) and GH-WA (crosses) methods.

$-5 \cdot 2^m$ and $k_2 = 2^m\lceil b \rceil = 5 \cdot 2^m$. When $m = 0$, there are 11 quadrature points, with index k ranging from k_1 to k_2, that is, $k \in \{-5, -4, -3, -2, -1, 0, 1, 2, 3, 4, 5\}$. Figure 1 shows the collocation of the nodes and weights for the GH and SINC quadratures. For a fair comparison, we have plotted the pairs $\left(\frac{k}{2^m}, \frac{1}{2^m} f_Z\left(\frac{k}{2^m}\right)\right)$ of expression (45), and the pairs $\left(x_i, \frac{1}{\sqrt{2\pi}} w_i\right)$ of expression (26). The SINC quadrature requires the selection of parameters m, k_1, k_2 following Proposition 1, and a probabilistic approach to reduce the mass lost in the tails, thus having total control on the parameteres of the numerical method and the errors. The quadrature points and the weights are then readily computed, even if a large number of points was needed. For a GH quadrature, the only parameter we can select is the number of nodes N_{GH}. An error formula for the GH quadrature exists (see for example [23]), but it relies on differentiation, making it difficult to use in practice. Furthermore, the nodes of a GH quadrature are obtained numerically as the roots of a certain polynomial. Despite the nodes can be calculated and stored for posterior implementations and, according to the package documentation, the quadrature nodes and weights generated by `hermegauss` have been tested only up to degree 100, and higher degrees may be problematic.

The results of SINC-WA method are shown in Table 3, where we have included n, which accounts for the total number of SINC quadrature nodes, facilitating this way the comparison with GH-WA of Table 2. Upon analysis, we observe that, in terms of accuracy, our SINC-WA method performs similarly to GH-WA method, when it comes to compute the VaR and ES values. We assume that both methods have the same computational cost when they use the same number of nodes, provided that those from

Method	Parameters				Results	
	m	k_1	k_2	n	**VaR Error**	**ES Error**
SINC-WA	0	-5	5	11	2.3588×10^{-3}	7.1210×10^{-3}
	0	-6	6	13	2.3588×10^{-3}	7.0260×10^{-3}
	1	-10	10	21	2.3588×10^{-3}	7.9711×10^{-3}
	1	-12	12	25	2.3588×10^{-3}	7.0709×10^{-3}
	2	-20	20	41	2.3588×10^{-3}	9.2905×10^{-3}

Table 3: Relative errors for the VaR and ES for P0 under a Gaussian copula model using SINC-WA method. The total number of quadrature points is denoted by n.

GH-WA are not calculated in execution time.

6.1.2 t-copula model

In this section, we compute the risk measures of portfolio P0 under a one-factor t-copula model for the cases $\nu = 5$ and $\nu = 2$ degrees of freedom. As usual, MC is the benchmark. We have also employed the QTA-WA from [7] described in Section 5.2. This method involves a Gauss-Laguerre quadrature, and we therefore denoted by n the number of quadrature points used. We also present results about the GHGL-WA method of Section 5.1. The Gauss-Laguerre quadratures are calculated with the function `roots_genlaguerre` from Scipy's special package. The results from Table 4 show that neither the QTA-WA method nor the GHGL-WA method work out well for $\nu = 2$, where the relative errors are about 30%.

Method	Parameters			$\nu = 5$		Time	$\nu = 2$		Time
				VaR	**ES**		**VaR**	**ES**	
MC				0.358974	0.449388	143.6s	0.523845	0.626056	142.8
	n	N_{GH}	N_{GL}	**VaR Error**	**ES Error**		**VaR Error**	**ES Error**	
QTA-WA	25	—	—	1.6565×10^{-2}	3.9873×10^{-2}	13.8s	6.2995×10^{-1}	6.5449×10^{-1}	12.1
	40	—	—	5.6835×10^{-3}	1.7904×10^{-2}	22.2s	5.3301×10^{-1}	5.3366×10^{-1}	19.3
	60	—	—	8.4040×10^{-3}	1.3303×10^{-2}	33.6s	3.9506×10^{-1}	4.0267×10^{-1}	28.6
GHGL-WA	—	11	37	2.4267×10^{-4}	8.5127×10^{-3}	—	—	—	—
	—	11	41	2.4267×10^{-4}	6.1136×10^{-3}	—	—	—	—
	—	11	45	2.4267×10^{-4}	4.5290×10^{-3}	—	—	—	—
	—	11	49	2.4267×10^{-4}	3.4375×10^{-3}	—	—	—	—
	—	11	65	2.4267×10^{-4}	3.4615×10^{-3}	—	—	—	—
	—	13	45	2.4267×10^{-4}	4.5417×10^{-3}	—	—	—	—
	—	13	49	2.4267×10^{-4}	3.4615×10^{-3}	—	—	—	—
	—	11	61	—	—	—	3.1490×10^{-1}	2.8340×10^{-1}	—
	—	11	65	—	—	—	3.1490×10^{-1}	2.8318×10^{-1}	—
	—	11	69	—	—	—	3.1490×10^{-1}	2.8301×10^{-1}	—
	—	11	69	—	—	—	3.1490×10^{-1}	2.8289×10^{-1}	—
	—	11	73	—	—	—	3.1490×10^{-1}	2.8279×10^{-1}	—
	—	13	65	—	—	—	3.1490×10^{-1}	2.8319×10^{-1}	—

Table 4: Relative errors for the VaR and ES for P0 corresponding to the QTA-WA and GHGL-WA methods under a t-copula model for $\nu = 2, 5$. The CPU time is given in seconds.

We now set the parameters for SINC-WA method. In regard to the Gaussian distribution we have already seen in the previous section that values $m = 0$, $k_1 = -5$ and $k_2 = 5$ provide great accuracy for both risk measures. It is left to select $\tilde{m}$, $\tilde{k}_1$ and $\tilde{k}_2$, the parameters related to the chi-squared distribution. Proposition 3 with the choice $\epsilon = 10^{-5}$ gives $m > 1.19$, while the choice $\epsilon = 10^{-7}$ gives

$m > 1.45$, so we select $\tilde{m} = 2$. For $\alpha = 0.00001$ we get $a \approx 0.00977$ and $b \approx 37.391$ for $\nu = 5$. Then, $\tilde{k}_1 = 2^{\tilde{m}}\lfloor \ln(0.00977) \rfloor = -5 \cdot 2^{\tilde{m}} = -20$ and $\tilde{k}_2 = 2^{\tilde{m}}\lceil \ln(37.391) \rceil = 4 \cdot 2^{\tilde{m}} = 16$. For the sake of comparison we have also computed the risk measures values for other different sets of parameters. Table 5 shows the results for the SINC-WA method. As we can observe, for the same number of quadrature points, that is, $n = N_{\text{GH}}$ and $\tilde{n} = N_{\text{GL}}$, the SINC-WA approximation produces errors in the range of ten to one hunded times smaller than the GHGL-method for the Expected Shortfall. This highlights the important feature of SINC-WA being able to approximate much better the tails than QTA-WA and GHGL-WA methods. As a final remark, we comment on the computational time. When SINC-WA and GHGL-WA rely on the same number of quadrature points, we may assume that they require comparable CPU time. Nevertheless, as shown in Table 5, their execution time is significantly lower than that of both the QTA-WA and the MC approaches.

Method	**Parameters**								**Results**		**Time**
	m	$\tilde{m}$	k_1	k_2	$\tilde{k}_1$	$\tilde{k}_2$	n	$\tilde{n}$	**VaR Error**	**ES Error**	
SINC-WA	0	2	-5	5	-20	16	11	37	2.4267×10^{-4}	5.6408×10^{-4}	0.35
			-5	5	-20	20	11	41	2.4267×10^{-4}	5.6408×10^{-4}	0.45
			-5	5	-24	16	11	41	2.4267×10^{-4}	1.3780×10^{-4}	0.49
			-5	5	-24	20	11	45	2.4267×10^{-4}	1.3780×10^{-4}	0.48
			-5	5	-24	-24	11	49	2.4267×10^{-4}	1.3780×10^{-4}	0.57
			-5	5	-28	16	11	45	2.4267×10^{-4}	1.0308×10^{-4}	0.50
			-6	6	-20	16	13	37	2.4267×10^{-4}	5.2140×10^{-4}	0.61
			-6	6	-24	-24	13	49	2.4267×10^{-4}	9.5118×10^{-5}	0.78
			-6	6	-28	16	13	45	2.4267×10^{-4}	6.0397×10^{-5}	0.77

Table 5: Relative errors for the VaR and ES for P0 corresponding to the SINC-WA method under a t-copula model with $\nu = 5$. The CPU time is given in seconds.

In practice, when using the t-copula model, the number of degrees of freedom should be estimated. We know, however, that as the number of degrees of freedom increases, the distribution becomes more symmetric and resembles a normal distribution. The proposed SINC-WA method is able to adapt to this feature much better than the traditional Gaussian quadratures. We ilustrate this by considering two degrees of freedom. We keep the same scale parameter, and calculate the new truncation values. For $Y \sim \chi^2_\nu$ with $\nu = 2$ we have that,

$$P(Y \leq 10^{-5}) \approx \frac{0.00001}{2}, \qquad P(Y \geq 24.412) \approx 1 - \frac{0.00001}{2},$$

and we obtain $\tilde{k}_1 = 2^{\tilde{m}}\lfloor \ln\left(10^{-5}\right) \rfloor = -12 \cdot 2^{\tilde{m}}$, and $\tilde{k}_2 = 2^{\tilde{m}}\lceil \ln(24.412) \rceil = 4 \cdot 2^{\tilde{m}}$.

Results are shown in Table 6. In this case, SINC-WA can achieve relative errors one hundred times

Method	**Parameters**								**Results**	
	m	$\tilde{m}$	k_1	k_2	$\tilde{k}_1$	$\tilde{k}_2$	n	$\tilde{n}$	**VaR Error**	**ES Error**
SINC-WA	0	2	-5	5	-44	16	11	61	9.4748×10^{-3}	1.7523×10^{-2}
			-5	5	-48	16	11	65	7.6106×10^{-3}	9.2566×10^{-3}
			-5	5	-52	16	11	69	7.6106×10^{-3}	6.2177×10^{-3}
			-5	5	-52	20	11	73	7.6106×10^{-3}	6.2177×10^{-3}
			-5	5	-56	16	11	73	7.6106×10^{-3}	5.1007×10^{-3}
			-5	5	-60	16	11	77	7.6106×10^{-3}	4.6839×10^{-3}
			-6	6	-48	16	13	65	7.6106×10^{-3}	9.2339×10^{-3}

Table 6: Relative errors for the VaR and ES for P0 corresponding to the SINC-WA method under a t-copula model with $\nu = 2$.

smaller for the VaR as well as for the ES values that GHGL-WA and QTA-WA. The CPU time for all the

experiments is around one second. With two degrees of freedom, the chi-squared distribution is really right-skewed and it has a heavy left tail, most of the values cluster very close to zero, with a long thin tail stretching out. In particular around 39% of mass is between 0 and 2 and about 86% is between 0 and 8. This explains why increasing $\tilde{k}_2$ makes little or no effect in terms of relative errors, but decreasing $\tilde{k}_1$ has a clearly impact for the ES.

6.2 Multi-factor models

It is well established that quadrature methods are subject to the curse of dimensionality, meaning that the number of evaluation points required for multidimensional integration increases exponentially with the number of dimensions. Since computational cost scales directly with the number of points, the overall expense also grows exponentially. Consequently, quadrature methods are generally considered impractical for high-dimensional integration problems. However, it is noteworthy that in the case of the one-factor model under both the Gaussian copula and the t-copula a relatively small number of quadrature points was sufficient to achieve accurate results. This observation suggests that our quadrature SINC-based approach may remain viable for multi-factor models, provided the number of dimensions remains moderate. In what follows, we consider a multi-factor model with a low number of factors, and implement a multi-dimensional quadrature scheme based on the sinc function, generalizing the method described in Section 5.3. For a large number of factors, we propose in Section 6.2.3 to obtain the characteristic function by simulation, and we call this method QMC-WA.

6.2.1 Gaussian copula model

We consider for the experiments the two portfolios given in Table 7. The dependence structure in this section is given by a three-factor Gaussian copula model as it was defined in Section 2.1. The loading factor matrix A has been generated randomly. Following similar arguments as in Section 5.3.1, we can

Portfolio	**N**	$\|\boldsymbol{A}\|_\infty$	$\boldsymbol{E}_n$	$\boldsymbol{P}_n$	**HHI**
P1	100	1.343	$C \cdot \frac{1}{n}$	0.01	0.061
P2	1000	1.464	$C \cdot \frac{1}{n}$	0.01	0.029

Table 7: Portfolio P1 and P2. The constant C is calculated such that $\sum_{j=1}^{N} E_j = 1$. MC is run with a sample size of 10^7 for the systematic factor $\mathbf{Z}$.

obtain an approximation of the characteristic function (12) given by,

$$\bar{\varphi}_L(\omega) := \frac{1}{2^{3m}} \sum_{k=k_1}^{k_2} \sum_{l=k_1}^{k_2} \sum_{s=k_1}^{k_2} f_{Z_1}\left(\tfrac{k}{2^m}\right)\, f_{Z_2}\left(\tfrac{t}{2^m}\right)\, f_{Z_3}\left(\tfrac{s}{2^m}\right) g\left(\left(\frac{k}{2^m}, \frac{l}{2^m}, \frac{s}{2^m}\right); \omega\right), \tag{68}$$

where g is defined in (11). Note that, since all the factors follow the same distribution we have already selected the same scale parameter m and same truncation parameters k_1 and k_2 for the three integrals corresponding to the three factors. Taking into account that, note also that the values $f_{Z_i}\left(\frac{k}{2^m}\right)$ are computed just once for all three factors.

In this case, we can compare our results with the QTA-WA method. As pointed out in [10], the QTA approach for the characteristic function, works out well for moderate correlation among obligors, that is, when $\|A\|_\infty = \max_j \sum_k |a_{jk}|$ is small. The rationale behind is that the accuracy of the approximation depends on the goodness of fit of the quadratic approximation. When the norm is not small, accuracy problems will arise. To overcome this problem, the authors of [10] proposed first to assume, without loss of generality, that the loading matrix A is structured so that its first column carries most of the loadings, meaning that the first factor affects most obligors. Then, the QTA method is applied to compute the conditional expectation with respect to that factor along with numerical integration (a quite time-consuming step) to uncondition with respect to that factor. In contrast, our methodology does not depend on the magnitude of this norm and can be applied to any loading factor matrix. To remark this comparison between the two methods, the two portfolios considered present a considerable norm as we can observe in Table 7.

For the experiments, the scale parameter m and the truncation values k_1 and k_2 were choosen as in Section 6.1.1, namely $m = 0, k_1 = -5, k_2 = 5$. These values already suffice to produce accurate estimates for the VaR and ES values. However, as in the previous examples, we provide additional results for other range of values for k_1 and k_2. The results in Table 8 show that all SINC-WA configurations produce highly accurate estimates for both VaR and ES across both portfolios, relative errors are below 1% for VaR values, while for the ES errors can be reduced by just a simple parameter tuning. Moreover, SINC-WA remains robust and accurate even in settings where the QTA-WA methodology fails, particularly for tail-risk metrics in more complex portfolios. We also report the computational times of all approaches. The SINC-WA method offers an excellent trade-off, delivering accurate risk measures with a drastic reduction in runtime with respect to MC, even for medium-sized portfolios. Meanwhile, QTA-WA, although fast, suffers from significant accuracy degradation. This underscores the advantage of the SINC-WA method as a reliable and efficient alternative for computing risk measures in credit portfolio models.

Method	**Parameters**			**P1**		**Time**	**P2**		**Time**
				VaR	**ES**		**VaR**	**ES**	
MC				0.301448	0.346223	118.0	0.244020	0.287758	264.4
	m	k_1	k_2	**VaR Error**	**ES Error**		**VaR Error**	**ES Error**	
QTA-WA				1.2694×10^{-1}	3.0505×10^{-1}	0.74	1.8960×10^{-1}	9.2008×10^{-1}	7.11
SINC-WA	0	-4	4	9.1255×10^{-3}	5.1653×10^{-2}	0.91	1.5082×10^{-3}	1.2543×10^{-1}	11.6
SINC-WA	0	-5	5	2.6464×10^{-3}	7.1421×10^{-3}	1.58	9.5121×10^{-3}	6.7703×10^{-2}	15.4
SINC-WA	0	-6	6	2.6464×10^{-3}	6.9622×10^{-3}	2.54	9.5121×10^{-3}	6.7468×10^{-2}	24.2

Table 8: VaR and ES relative errors for the QTA-WA and SINC-WA methods. The CPU time is given in seconds.

6.2.2 t-copula model

We consider a two-factor t-copula model as in expression (7). We can approximate the characteristic function (18) as,

$$\tilde{\tilde{\varphi}}_L(\omega) := \frac{1}{2^{2m}} \cdot \frac{1}{2^{\tilde{m}}} \cdot \frac{1}{2^{\nu/2}\Gamma\left(\frac{\nu}{2}\right)} \sum_{k=k_1}^{k_2} \sum_{l=k_1}^{k_2} \sum_{s=\tilde{k}_1}^{\tilde{k}_2} f_{Z_1}\left(\frac{k}{2^m}\right) f_{Z_2}\left(\frac{l}{2^m}\right) f\left(\frac{s}{2^{\tilde{m}}}\right) g\left(\left(\frac{k}{2^m}, \frac{l}{2^m}, e^{\frac{s}{2^{\tilde{m}}}}\right); \omega\right). \quad (69)$$

We consider the same portfolios defined in Table 7, although the norms change because of the fact that we have one factor less. In particular, for P1 we have $||A||_\infty = 0.935$, whereas for P2 we have $||A||_\infty = 0.980$. The factor loadings are randomly generated as before. We compute the risk measures with the QTA-WA method, being MC the benchmark. Table 9 presents the results when $\nu = 3$, where n denotes again the number of nodes used in the Gauss–Laguerre quadrature within the QTA-WA method. For portfolio P2, the method was only applied with a small number of quadrature nodes, since its computational complexity increases rapidly with the number of nodes considered.

Results for the SINC-WA method are shown in Table 10. With $\nu = 3$, we select $\tilde{m} = 2$ and the truncation points a and b such that,

$$P(Y \leq a) = \frac{0.00001}{2}, \quad \text{and,} \quad P(Y \geq b) = 1 - \frac{0.00001}{2},$$

where $Y \sim \chi^2_3$. We obtain $a \approx 0.000707, b \approx 27.338$, $\tilde{k}_1 = 2^{\tilde{m}}\lfloor \ln(0.000707) \rfloor = -8 \cdot 2^{\tilde{m}} = -32$ and $\tilde{k}_2 = 2^{\tilde{m}}\lceil \ln(27.338) \rceil = 4 \cdot 2^{\tilde{m}} = 16$. As we have already seen in former examples, increasing the value of the truncation parameters, does not affect the results, since an extremely small part of the density mass is set aside, that is way we omit some computations for P2. All in all, the SINC-WA method achieves an impressive reduction in the relative error in the range of 10 to 10^4 when compared to QTA-WA, where this last method gives nonsensical results.

Method	Parameters	P1		Time	P2		Time
		VaR	ES		VaR	ES	
MC		0.533292	0.617591	141.3	0.493251	0.573785	284.1
	n	VaR Error	ES Error		VaR Error	ES Error	
QTA-WA	25	1.6040×10^{-1}	1.8421×10^{-1}	14.3	2.0905×10^{-1}	1.8213×10^{-1}	163.1
	40	8.7148×10^{-2}	8.2861×10^{-2}	22.9	—	—	—
	50	6.7005×10^{-2}	5.2704×10^{-2}	27.1	—	—	—
	60	9.5880×10^{-1}	1.1121×10^{1}	32.0	6.3472×10^{-1}	2.2637×10^{0}	366.6

Table 9: VaR and ES relative errors for the QTA-WA method. The CPU time is given in seconds.

Method	Parameters								P1		Time	P2		Time
	m	$\tilde{m}$	k_1	k_2	$\tilde{k}_1$	$\tilde{k}_2$	n	$\tilde{n}$	VaR Error	ES Error		VaR Error	ES Error	
SINC-WA	0	2	-5	5	-32	16	11	49	2.5803×10^{-3}	3.5510×10^{-3}	6.77	2.794×10^{-3}	1.825×10^{-2}	65.2
			-5	5	-32	20	11	53	2.5803×10^{-3}	3.5510×10^{-3}	8.38	—	—	—
			-5	5	-36	16	11	53	2.5803×10^{-3}	1.6818×10^{-3}	7.23	8.139×10^{-4}	1.606×10^{-2}	73.7
			-5	-5	-36	20	11	57	2.5803×10^{-3}	1.6818×10^{-3}	7.76	—	—	—
			-5	-5	-40	16	11	57	2.5803×10^{-3}	1.2656×10^{-3}	7.73	8.139×10^{-4}	1.557×10^{-2}	78.2
			-5	-5	-44	16	11	61	2.5803×10^{-3}	1.1728×10^{-3}	8.22	8.139×10^{-4}	1.547×10^{-2}	83.9
			-6	-6	-32	16	13	49	2.5803×10^{-3}	3.5055×10^{-3}	9.23	—	—	—

Table 10: VaR and ES relative errors for SINC-WA method with respect to MC values. CPU time is given in seconds.

6.2.3 Large number of factors: the QMC-WA method

When the number of factors is large or when the size of the portfolio is big, quadrature methods become computationally impractical. In such cases, we propose to compute the characteristic function based on a simulation approach suitable for multi-factor models with an arbitrary number of factors. Although we focus on the Gaussian copula, this approach can also be easily extended to the t-copula model. Specifically, given the expression (12) that defines the characteristic function of the Gaussian copula model, we generate a quasi-Monte Carlo sample from a multivariate normal distribution by means of Sobol sequences (we use the function `Sobol` from the Scipy's Quasi-Monte Carlo submodule). This approach proves to be highly efficient with a small sample size, performing at least as well as the QTA-WA method in the Gaussian setting, and significantly better in cases where QTA-WA fails to yield reliable results. The test portfolios for the numerical experiments in this section are shown in Table 11.

Portfolio	N	d	$\|A\|_\infty$	E_n	P_n	HHI
P3	1000	6	0.518	$C \cdot \frac{1}{n}$	0.01	0.029
P4	10000	3	0.287	$C \cdot \frac{1}{n}$	0.01	0.017
P5	100	8	0.653	$C \cdot \frac{1}{n}$	0.01	0.061
P6	1000	5	2.225	$C \cdot \frac{1}{n}$	0.01	0.029

Table 11: Portfolios P3, P4, P5 and P6. The constant C is calculated such that $\sum_{j=1}^{N} E_j = 1$. MC is run with a sample size of 10^7 for the systematic factor $\mathbf{Z}$, where d denotes the dimension of $\mathbf{Z}$.

The loading matrix is computed randomly generating uniform numbers from 0 to 1. For P3, P4, P5 we generate the factor loadings as $A = 0.1 \cdot \text{random}(N, d)$, while for P6 we have set $A = 0.5 \cdot \text{random}(N, d)$. As usual, we will use the inversion method based on Haar wavelets, so we denote the proposed method by QMC-WA. In the first experiment, we have considered different scale parameters m for the Haar inversion method. The sample size has been set to 128 Sobol points for the first three portfolios. As we can observe in Table 12, overall our methodology delivers the same level of relative accuracy as the QTA-WA method, but in a shorter computational time, with the benefit of using a small random sample.

Moreover, across all tested portfolios, our method is substantially faster than a standard MC simulation providing also great accuracy in terms of relative error. In what follows, we will consider the scale of

Method	Parameters	P3		Time	P4		Time	P5		Time
		VaR	ES		VaR	ES		VaR	ES	
MC		0.153658	0.170937	274.8	0.119391	0.132389	1535.4	0.216069	0.241581	117.6
	m	VaR Error	ES Error		VaR Error	ES Error		VaR Error	ES Error	
QTA-WA	8	4.1551×10^{-3}	3.9875×10^{-1}	1.64	2.0983×10^{-3}	1.8547×10^{-1}	15.5	3.3687×10^{-3}	1.3659×10^{-1}	0.17
	9	1.0511×10^{-2}	4.0434×10^{-2}	2.95	6.0813×10^{-3}	1.5400×10^{-2}	34.7	1.1510×10^{-3}	3.6641×10^{-2}	0.40
	10	9.7739×10^{-4}	5.3311×10^{-3}	6.95	1.9915×10^{-3}	1.1740×10^{-3}	111.8	5.6296×10^{-3}	1.2656×10^{-2}	0.74
QMC-WA	8	4.1551×10^{-3}	3.9493×10^{-1}	0.38	2.0983×10^{-3}	1.8789×10^{-1}	15.2	3.3687×10^{-3}	1.3573×10^{-1}	0.20
	9	1.0511×10^{-2}	3.9245×10^{-2}	0.78	6.0813×10^{-3}	1.4996×10^{-2}	30.8	1.1510×10^{-3}	3.7910×10^{-2}	0.29
	10	7.3328×10^{-3}	8.0543×10^{-3}	1.43	1.9915×10^{-3}	8.1149×10^{-4}	61.3	5.6296×10^{-3}	1.1950×10^{-2}	0.53

Table 12: Relative errors for the VaR and ES computation for QTA-WA and QMC-WA methods. The CPU time is measured in seconds.

approximation $m = 10$ of the WA inversion method. An error analysis about the selection of the scale can be found in [7].

We note that we have used a small sample to get accurate results with the QMC-WA method. In order to assess the influence of that sample on the results, we have repeated the calculation of risk measures ten times, each with an independent random sample, and computed the maximum and minimum relative error obtained for the ten iterations. As shown in Table 13, the relative errors remain well-controlled, where lower bounds are smaller than those previously observed.

Method	P3		P4		P5	
	VaR Error	ES Error	VaR Error	ES Error	VaR Error	ES Errors
QMC-WA	$7.333 \times 10^{-3}, 9.7739 \times 10^{-3}$	$3.937 \times 10^{-3}, 1.082 \times 10^{-2}$	$1.992 \times 10^{-3}, 1.992 \times 10^{-3}$	$1.759 \times 10^{-3}, 2.352 \times 10^{-3}$	$1.109 \times 10^{-3}, 5.629 \times 10^{-3}$	$9.961 \times 10^{-3}, 1.046 \times 10^{-2}$

Table 13: Minimum and maximum relative errors for the VaR and the ES for 10 independent iterations.

As discussed earlier in Section 6.2.1, the QTA-WA method exhibits a decline in accuracy as the norm of the loading factor matrix increases. To illustrate this limitation, we consider portfolio P6, which is characterized by a large norm. Table 14 reports the relative errors for the VaR and ES obtained using the QTA-WA approach, as well as the minimum and maximum errors across ten independent runs of the QMC-WA method with 128 Sobol points, all measured with respect to the MC benchmark. The results highlight the suboptimal performance of both methods. Notably, the QTA-WA method yields a negative value for the ES, which lacks of meaningful interpretation. With the sample size set as 128 Sobol points, the QMC-WA approach shows a wide range of errors across different iterations, in some cases of similar magnitude to those observed with the QTA-WA method, although it runs in considerably less time (the CPU time shown in the table is for one iteration).

Method	P6		Time
	VaR	ES	
MC	0.288974	0.350445	273.3
	VaR Error	ES Error	
QTA-WA	3.8664×10^{-1}	5.7313×10^{0}	7.12
QMC-WA	$7.2964 \times 10^{-2}, 4.1766 \times 10^{-1}$	$4.4251 \times 10^{-2}, 3.1212 \times 10^{-1}$	1.46

Table 14: VaR and ES relative errors for QTA-WA and QMC-WA methods. CPU time is measured in seconds.

For our methodology, we propose to increase the sample size up to 1024 Sobol points, and show the results in Table 15. This comes at the expense of an increase of computational time, as generating and managing low-discrepancy sequences, especially in high-dimensional spaces, can be more complex and

computationally intensive than using standard random sampling, but the method is still faster than a crude MC scheme, and it provides much more accurate results than the QTA-WA method for both the VaR and the ES.

	P6									
	Iter 1	**Iter 2**	**Iter 3**	**Iter 4**	**Iter 5**	**Iter 6**	**Iter 7**	**Iter 8**	**Iter 9**	**Iter 10**
VaR Error	1.0277e-01	5.9446e-02	8.6481e-02	2.5652e-02	9.6007e-02	5.3754e-03	1.3835e-03	5.5454e-02	1.6083e-01	3.9170e-02
ES Error	5.2243e-02	1.5152e-01	9.9545e-02	9.2381e-02	9.8690e-02	1.5285e-01	7.2329e-02	1.5263e-02	5.1804e-01	7.3269e-02
CPU Time	45.43 per iteration									

Table 15: VaR and ES relative errors for 10 iterations with 1024 Sobol points. The CPU time is measured in seconds, and it corresponds to one iteration.

6.3 Porfolio with real data and climate factors

We now consider a portfolio with real data. Specifically we use a portfolio with data retrieved on March 31, 2025 from the EIB (`www.eib.org`) corresponding to 4,251 loans issued by the bank all over the world. The total nominal amount of these loans is around 360,683 millions of euros. The selected subset corresponds to loans categorized under the label of *loans for the public sector*, meaning that they were granted to sovereign states, national agencies, departments, institutions and ministries, regional or local authorities or public sector companies. For each loan the available information is the name of the company the loan was granted to, the associated region and country (or territory), sector in which the company operates, the signature date, the signed amount of the loan and a short description of the project to which the loan is associated. We have further filtered the database as follows.

- We first drop the loans that have a region but not a country associated.
- We need a probability of default for each obligor, and we therefore proceed as follows. Since each loan is linked to a specific country, we will assign to each loan the rating of the corresponding country downloaded from `https://datosmacro.expansion.com/ratings` on March 31, 2025. Loans associated with countries that either lack a rating or have a 'NR' (not rated) qualification will be excluded. Next, to translate the rating to a default probability we use the sovereign foreign currency average one-year transition rates from each rating to SD (selective default) rating available in [21]. As not all rating categories are available, we interpolate the missing transition probabilities. Table 16 shows the interpolated transition probabilities from every rating category to SD rating.
- Looking at the exposure of the loans, we decided to remove those loans from countries that belong to the regions EFTA countries, South Africa, Eastern Europe, Mediterranian and Caribbean with a negligible relative exposure with respect to the total amount (7 loans associated with 2 countries in the Caribbean region, and 71 loans associated to 6 countries in the Mediterranean and Eastern Europe regions). A summary of loans and exposure is presented in Table 17.

Finally, the database is composed of 3,648 loans that amount around 337,100 millions of euros.

We consider two Gaussian copula models composed of a different number of systematic factors and they will be called M1 and M2. The first model M1, is composed of a global economic factor, a global physical risk factor, and a global transition risk factor, resulting in a three-factor model. For M2, we consider a global economic factor, a global transition factor, and a physical risk factor for each of the following continents, Asia, Europe, Africa, and Central and Latin America, leading to a model with a total of six factors.

The next step is to assign the factor loadings for every loan with respect to each risk factor. The assigment is based on the following criteria.

- The economic risk factor accounts for all the external and macroeconomic variables such as inflation or interest rates that can influence the creditworthiness of borrowers. Different regions have different sensitivities to these global shocks, developed Europe is more integrated with global markets, hence the factor loadings should be higher whereas emerging african or asian countries are

Rating	Reported S&P	Interpolated transition probabilities
AAA	0.00	0.001*
AA+		0.0055
AA	0.00	0.01*
AA-		0.04
A+		0.07
A	0.00	0.1*
A-		0.123
BBB+		0.147
BBB	0.14	0.17
BBB-		0.227
BB+		0.283
BB	0.41	0.340
BB-		0.110
B+		0.186
B	2.90	2.62
B-		12.163
CCC+		21.707
CCC	30.47	31.250
CCC-		40.793
CC		50337
C		59.880
SD		69.423

Table 16: Column *Reported S&P* reports the one-year transition rates (in %) from selected sovereign foreign currency credit ratings to the SD rating, given by Standard & Poor's in [21]. Probabilities marked with * have been manually set before the interpolation in order to get not null estimated probabilities.

Region	Number of loans	Exposure	Final number of loans	Final exposure
European Union	3297	91.38	3297	93.00
Africa, Caribbean, Pacific countries + OCT	89	1.02	82	0.97
Enlargement Countries	81	1.38	81	1.40
Asia and Latin America	82	2.13	82	2.17
Mediterranean countries	79	2.78	43	1.85
Eastern Europe, Southern Caucasus	98	0.91	63	0.61
EFTA countries	11	0.21	-	-
South Africa	7	0.19	-	-

Table 17: Number of loans and relative exposure (in %) for every given region in our portfolio.

usually more driven by local and idiosyncratic conditions, hence a lower loading factor should be contemplated. Table 18 summarizes this assignment.

Region	Factor loadings
European countries	0.5
Asian countries	0.3
African countries	0.2
Central & South America	0.3

Table 18: Factor loadings corresponding to the global economic factor.

- To assign the factor loadings corresponding to the transition risk factor, we take into account that every loan falls into one of the following sectors, credit lines, water and sewerage, energy, industry, urban development, education, health, transport, agriculture fisheries and forestry, telecom, services, solid waste or composite infrastructure. Obviously, some economic sectors such as the energy

sector or agriculture fisheries and forestry sector are more expose and vulnerable to environmental fluctuations, and climate change has a higher impact than in other sectors, due to their direct dependence on natural resources and ecosystems. Table 19 shows the factor loadings.

Sector	**Factor loadings**	**Sector**	**Factor loadings**
Credit lines	0.1	Transport	0.4
Water, sewerage	0.4	Agriculture, fisheries, forestry	0.4
Energy	0.5	Telecom	0.1
Industry	0.4	Services	0.2
Urban development	0.4	Solid waste	0.4
Education	0.2	Composite infrastructure	0.3
Health	0.2		

Table 19: Factor loadings corresponding to the global transition risk factor.

- Finally, to set the factor loadings corresponding to the physical risk factors associated with the borrower's country, we employ the Climate Risk Index published by Germanwatch, a human rights organization located in Germany that, since 2006, reports an index that measure how extreme weather events affect countries. In particular, in this work, we will use the normalized (between 0 and 1) Climate Risk Index 2022 from [2]. In particular, in our portolio, the greatest factor loading is 0.559, corresponding to loans given to companies based in Italy, as this country ranks third in the Climate Risk index. In the first model, this normalized index will be used as a measure of the loadings between the loan and climate change-related physical risk factors worldwide. In contrast, for the second model, this loading is restricted to the relationship between the loan and the physical risk factor specific to the continent the loan is indexed to.

The resulting factor loadings matrix has 3,648 rows and either 3 or 6 columns, depending on if we are considering M1 or M2, respectively. Its norm is 1.559 in both cases, since there is only one non-zero factor loading per obligor corresponding to the continent to which the loan belongs. We first compute the VaR and ES values for the three-factor model. As the dimension is moderate we will use the SINC-WA method. The results are shown in Table 20. Despite being faster, QTA-WA is less reliable than SINC-WA, since the relative errors are above 50% for both risk measures. On the other hand, the SINC-WA produces accurate risk estimates for both the VaR and ES, making it a trustworthy method for risk assessment. Despite taking more time than QTA-WA, it clearly outperforms MC in terms of computational efficiency.

Method	**Parameters**			**M1**		**Time**
				VaR	**ES**	
MC				0.090066	0.134369	641.9
	m	k_1	k_2	**VaR Error**	**ES Error**	
QTA-WA				5.2834×10^{-1}	6.5029×10^{-1}	25.9
SINC-WA	0	-5	5	4.0415×10^{-2}	1.0577×10^{-3}	57.3
	0	-6	6	4.0415×10^{-3}	4.5969×10^{-4}	79.0
QMC-WA				8.3786×10^{-2}	1.3632×10^{-2}	161.2

Table 20: VaR and ES relative errors for the three-factor Gaussian copula model M1. The CPU time is measured in seconds.

To conclude this work, we compute the risk measures for the six-factor Gaussian copula model M2. The results, shown in Table 21, obtained from two independent runs of the QMC-WA approach indicate that, although the QMC-WA method continues to display non-negligible errors, these errors are

consistently smaller than those observed under the QTA-WA method, confirming its superior robustness and reliability for loading matrices with big norms, where the QTA-WA method tend to fail. This relative improvement highlights the potential of QMC-based techniques as we have also seen in Section 6.2.3. It is worth remarking that the portfolio composition introduces additional complexities, since following Table 17, approximately 91% of the exposure is concentrated in European countries. This imply that most of the factor loadings for the physical risk factors associated with Asian, African and Central and South America are zero, making a very sparse factor loadings matrix. This combination of methodological limitations and portfolio features makes the accurate quantification of risk particularly challenging.

Method	**M2**		**Time**
	VaR	**ES**	
MC	0.088941	0.132673	739.1
	VaR Error	**ES Error**	
QTA-WA	5.2238×10^{-1}	6.4582×10^{-1}	24.2
QMC-WA	2.8281×10^{-2}	3.0519×10^{-1}	163.4
QMC-WA	1.6936×10^{-1}	1.5480×10^{-2}	161.2

Table 21: VaR and ES relative errors for the six-factor Gaussian copula model M2. CPU time is measured in seconds.

7 Conclusions

In this paper we have presented a new numerical method called SINC-WA for computing the characteristic function of the credit loss distribution under a one-factor credit risk model, based on the sinc function. The results show an impressive accuracy and execution time when compared to its competitors for the regulatory Gaussian copula model as well as for the t-copula model. An error analysis provide the recipe to determine the parameters of SINC-WA beforehand, which makes it more reliable and useful in practice. The proposed method is successfully extended to multi-factor Gaussian and t-copula models, when a moderate number of factors are considered. In all the presented cases, our methodology outperforms the current state-of-the-art methods, such as the QTA-WA and traditional Gaussian-Hermite and Gaussian-Laguerre quadratures. Furthermore, for the multi-factor Gaussian copula model for high number of risk factors, when quadratures can not be applied because of the curse of dimensionality, we propose a simulation method based on low-discrepancy sequences to compute the characteristic function, which still achieves great accuracy and speed. Future work could be focused on computing the risk contributions, and exploring the possibility of estimating the factor loadings from real data.

Funding

We acknowledge support from the Departament de Recerca i Universitats, the Departament d'Acció Climàtica, Alimentació i Agenda Rural, and the Fons Climàtic of the Generalitat de Catalunya (2023 CLIMA 00012).

Data availability statement

The data used in this work is of public access, and it is available upon request to the authors.

References

[1] M. Abramowitz and I.A. Stegun. *Handbook of mathematical functions: with formulas, graphs, and mathematical tables*. 1965.

[2] L. Adil et al. *Climate risk index 2025: who suffers most from extreme weather events?* In: *Available at www.germanwatch.org* (2025).

[3] Basel Committee on Banking Supervision. *Basel III: Finalising post-crisis reforms*. In: *Available at www.bis.org* (2017).

[4] Basel Committee on Banking Supervision. *International convergence of capital measurement and capital standards: A revised framework - Comprehensive version*. In: *Available at www.bis.org* (2006).

[5] E. Campiglio et al. *Climate change challenges for central banks and financial regulators*. In: *Nature climate change* 8.6 (2018), pp. 462–468.

[6] C. Cattani. *Shannon wavelets theory*. In: *Mathematical Problems in Engineering* 2008.1 (2008), pp. 91–114.

[7] G. Colldeforns-Papiol, L. Ortiz-Gracia, and C.W. Oosterlee. *Quantifying credit portfolio losses under multi-factor models*. In: *International journal of computer mathematics* 96.11 (2019), pp. 2135–2156.

[8] J. Garnier, J.-B. Gaudemet, and A. Gruz. *The climate extended risk model (CERM)*. In: *Available at www.arxiv.org* (2022).

[9] P. Glasserman, W. Kang, and P. Shahabuddin. *Large deviations in multifactor portfolio credit risk*. In: *Mathematical finance* 17.3 (2007), pp. 345–379.

[10] P. Glasserman and S. Suchintabandid. *Quadratic Transform Approximation for CDO Pricing in Multifactor Models*. In: *SIAM journal on financial mathematics* 3.1 (2012), pp. 137–162.

[11] A. Leitao, L. Ortiz-Gracia, and E.I. Wagner. *SWIFT valuation of discretely monitored arithmetic Asian options*. In: *Journal of computational science* 28 (2018), pp. 120–139.

[12] Eva Lütkebohmert. *Concentration risk in credit portfolios*. Springer, 2009.

[13] S.C. Maree, L. Ortiz-Gracia, and C.W. Oosterlee. *Pricing early-exercise and discrete barrier options by Shannon wavelet expansions*. In: *Numerische Mathematik* 136.4 (2017), 1035–1070.

[14] R. Martin and T. Wilde. *Unsystematic credit risk*. In: *Risk* 15 (2002), pp. 123–128.

[15] J.J. Masdemont and L. Ortiz-Gracia. *Haar wavelets-based approach for quantifying credit portfolio losses*. In: *Quantitative Finance* 14 (2014), pp. 1587–1595.

[16] A.J. McNeil, R. Frey, and P. Embrechts. *Quantitative risk management : concepts, techniques and tools*. Revised edition. Princeton series in finance. Princeton University Press, 2015. ISBN: 0691166277.

[17] L. Ortiz-Gracia and J.J. Masdemont. *Credit risk contributions under the Vasicek one-factor model: A fast wavelet expansion approximation*. In: *Journal of Computational Finance* 17.4 (2014), pp. 59–97.

[18] L. Ortiz-Gracia and J.J. Masdemont. *Peaks and jumps reconstruction with B-splines scaling functions*. In: *Journal of computational and applied mathematics* 272 (2014), pp. 258–272.

[19] L. Ortiz-Gracia and C.W. Oosterlee. *Robust Pricing of European Options with Wavelets and the Characteristic Function*. In: *SIAM Journal on Scientific Computing* 35.5 (2013), B1055–B1084.

[20] M. Pykhtin. *Multi-factor Adjustment*. In: *Risk* 17 (2004), pp. 85–90.

[21] S&P Global Ratings. *Default, Transition, and Recovery: 2024 Annual Global Sovereign Default and Rating Transition Study*. In: *Available at www.spglobal.com/ratings* (2024).

[22] F. Stenger. *Handbook of Sinc Numerical Methods*. 1st ed. Chapman & Hall/CRC numerical analysis and scientific computing. CRC Press, 2011. ISBN: 9781439821589.

[23] E. Süli and D.F. Mayers. *An introduction to numerical analysis*. 1st ed. Cambridge University Press, 2003. ISBN: 1-107-13229-0.

UBIREA
Institut de Recerca en Economia Aplicada Regional i Pública
Research Institute of Applied Economics
Universitat de Barcelona
Av. Diagonal, 690 • 08034 Barcelona

WEBSITE: www.ub.edu/irea/ • **CONTACT:** irea@ub.edu